NAVAL POSTGRADUATE SCHOOL

MONTEREY, CALIFORNIA

THESIS

NUMERICAL STUDY OF THE EFFECT OF THE FUEL FILM ON HEAT TRANSFER IN A ROCKET ENGINE COMBUSTION CHAMBER

by

Goh,Sing Huat Patrick

December 2003

Thesis Advisor:	Ashok Gopinath
Co-Advisor:	Christopher Brophy

THIS PAGE INTENTIONALLY LEFT BLANK

REPORT DOCUMENTATION PAGE			Form Approved OMB No. 0704-0188
Public reporting burden for this collection of information is estimated to average 1 hour per response, including the time for reviewing instruction, searching existing data sources, gathering and maintaining the data needed, and completing and reviewing the collection of information. Send comments regarding this burden estimate or any other aspect of this collection of information, including suggestions for reducing this burden, to Washington headquarters Services, Directorate for Information Operations and Reports, 1215 Jefferson Davis Highway, Suite 1204, Arlington, VA 22202-4302, and to the Office of Management and Budget, Paperwork Reduction Project (0704-0188) Washington DC 20503.			
1. AGENCY USE ONLY *(Leave blank)*	**2. REPORT DATE** December 2003	**3. REPORT TYPE AND DATES COVERED** Master's Thesis	
4. TITLE AND SUBTITLE: Numerical Study Of The Effect Of The Fuel Film On Heat Transfer In A Rocket Engine Combustion Chamber		**5. FUNDING NUMBERS**	
6. AUTHOR(S) GOH, SING HUAT			
7. PERFORMING ORGANIZATION NAME(S) AND ADDRESS(ES) Naval Postgraduate School Monterey, CA 93943-5000		**8. PERFORMING ORGANIZATION REPORT NUMBER**	
9. SPONSORING /MONITORING AGENCY NAME(S) AND ADDRESS(ES) N/A		**10. SPONSORING/MONITORING AGENCY REPORT NUMBER**	
11. SUPPLEMENTARY NOTES The views expressed in this thesis are those of the author and do not reflect the official policy or position of the Department of Defense or the U.S. Government.			
12a. DISTRIBUTION / AVAILABILITY STATEMENT Approved for public release; distribution is unlimited.		**12b. DISTRIBUTION CODE**	

13. ABSTRACT ***(maximum 200 words)***

The combustion chamber of a liquid-fueled rocket engine with an injected fuel film on the wall has been numerically simulated. The engine has been modeled to operate on an RP-1/gaseous oxygen mixture at a chamber pressure of 35 atmospheres. The fuel is a hydrocarbon blend and is used for both engine operation and the fuel-film layer. The fuel layer acts as a flowing thermal insulating shield, reducing the amount of convective and radiative heat flux from the hot combustion gases to the chamber wall. This effort evaluates the effectiveness of the fuel layer in achieving the reduced heat flux to the chamber wall under varying emission/absorption conditions. The tendency of hydrocarbon fuels to produce soot precipitates at near 550K directly affects the optical properties of the fuel layer and the resulting heat transfer to the wall has been modeled and discussed.

14. SUBJECT TERMS Heat transfer, Rocket engine, Combustion chamber, film cooling, RP1, Absorption coefficient, RADCAL, TEP, CFDACE			**15. NUMBER OF PAGES** 89
			16. PRICE CODE
17. SECURITY CLASSIFICATION OF REPORT Unclassified	**18. SECURITY CLASSIFICATION OF THIS PAGE** Unclassified	**19. SECURITY CLASSIFICATION OF ABSTRACT** Unclassified	**20. LIMITATION OF ABSTRACT** UL

NSN 7540-01-280-5500

Standard Form 298 (Rev. 2-89)
Prescribed by ANSI Std. 239-18

THIS PAGE INTENTIONALLY LEFT BLANK

Approved for public release; distribution is unlimited

NUMERICAL STUDY OF THE EFFECT OF THE FUEL FILM ON HEAT TRANSFER IN A ROCKET ENGINE COMBUSTION CHAMBER

Goh, Sing Huat
Major, Singapore Armed Forces (Army)
B.Eng, National University of Singapore, 1998

Submitted in partial fulfillment of the
requirements for the degree of

**MASTER OF SCIENCE IN ENGINEERING SCIENCE
(MECHANICAL ENGINEERING)**

from the

**NAVAL POSTGRADUATE SCHOOL
December 2003**

Author: Goh, Sing Huat

Approved by: Ashok Gopinath
Thesis Advisor

Christopher Brophy
Co-Advisor

Anthony J. Healey
Chairman, Department of Mechanical and Astronautical Engineering

THIS PAGE INTENTIONALLY LEFT BLANK

ABSTRACT

The combustion chamber of a liquid-fueled rocket engine with an injected fuel film on the wall has been numerically simulated. The engine has been modeled to operate on a RP-1/gaseous oxygen mixture at a chamber pressure of 35 atmospheres. The fuel is a hydrocarbon blend and is used for both engine operation and the fuel-film layer. The fuel layer acts as a flowing thermal insulating shield, reducing the amount of convective and radiative heat flux from the hot combustion gases to the chamber wall. This effort evaluates the effectiveness of the fuel layer in achieving a reduced heat flux to the chamber wall under varying emission/absorption conditions. The tendency of hydrocarbon fuels to produce soot precipitates at near 550K directly affects the optical properties of the fuel layer and the resulting heat transfer to the wall has been modeled and discussed.

THIS PAGE INTENTIONALLY LEFT BLANK

TABLE OF CONTENTS

LIST OF FIGURES

THIS PAGE INTENTIONALLY LEFT BLANK

LIST OF TABLES

THIS PAGE INTENTIONALLY LEFT BLANK

ACKNOWLEDGMENTS

I would like to first thank God, my Lord Jesus Christ for the wisdom and strength blessed upon me in doing this thesis research.

I would also like to express my heartfelt appreciation to Associate Professor Ashok Gopinath for his continuous guidance and support throughout the work.

Special thanks and gratitude to Research Professor. Christopher Brophy for his inputs and advice given me during the course of work.

Lastly, but not the least, I thank my loving wife, Hannah, for her understanding, sacrifice, love and support, and my dear son Joshua, for adding so much joy in our lives.

THIS PAGE INTENTIONALLY LEFT BLANK

I. INTRODUCTION

The heat transfer analysis of hydrocarbon fuel rocket engine combustion chambers has many applications. Such an analysis can help determine important parameters such as chamber wall temperature. Due to material limitations, the chamber wall can only withstand a maximum operating temperature, beyond which, its material properties will deteriorate, resulting in possible catastrophic failure.

The other important application of heat transfer analysis, especially in hydrocarbon fuel rocket engines, is the process of creation of soot. Hydrocarbon fuels turn to soot at certain temperatures, and heat transfer analysis helps determine the soot conditions within the combustion chamber as well as the amount of soot discharged into the rocket exhaust plume, and hence the Infrared (IR) signature of the plume. This has important military / operational implications such as in signature detection or exposure.

This study is a part of research in Plume signature analysis of hydrocarbon fuel rocket engine sponsored by Air Force Research Laboratory. Other related theses/studies at the Naval Postgraduate School include the recent numerical effort by Savur [1], and the experimental study by Rochford.

The present study builds upon the numerical work done by Savur [1]. Savur [1] investigated the radiative contribution to the heat transfer rate from the hot participating chamber gases to the cooler chamber wall. His model comprised of the chamber wall with the hot gases flowing through the chamber. The current study further improves upon his model by introducing the presence of a thin layer of fuel on the chamber wall. This modification of the numerical model better represents the actual film-cooled rocket engine used in the

experiments. The aim of this study is to investigate the effect of the fuel layer on the heat transfer to the chamber wall and provide results for corroboration with experimental data. It will also investigate the coking phenomenon of the conversion of RP1 to soot within the combustion chamber and its impact on the heat transfer to the chamber wall.

II. DESCRIPTION OF LIQUID FUEL ROCKET ENGINE

A simple schematic diagram of a typical liquid fuel rocket engine is shown in Figure 1.

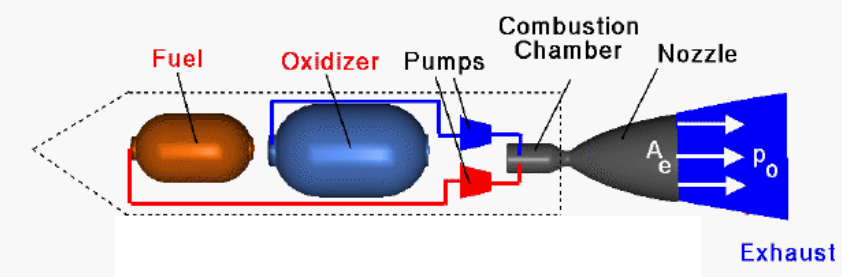

Figure 1. Schematic diagram of a typical liquid fuel rocket engine.

The liquid fuel is usually kerosene (RP1) and the oxidizer here is gaseous oxygen. The fuel and the oxidizer are pumped into the combustion chamber where they are mixed and ignited. The combustion process builds up high temperatures and pressures within the combustion chamber. The expanding gas then escapes through the nozzle and then out into the exhaust plume.

The interest in the study is the heat transfer within the combustion chamber, which has very high temperature and pressure. Of special concern in the study is the material and structural limitation of the chamber wall as it absorbs heat from the hot combustion gases. Shown in Table 1 are some of the typical materials used for combustion chambers and their melting temperatures.

Material	Melting Temp (K)
Stainless Steel 304	1713.15
Monel 400	1597
Hasteloy X	1580
Copper (OFHC)	1356

Data courtesy of High Performance Alloys Inc

Table 1. Typical materials for combustion chamber and their melting temperatures

A. COOLING OF COMBUSTION CHAMBER

The primary objective of cooling is to prevent the chamber from becoming too hot, so that it will no longer be able to withstand the imposed loads or stresses, thus causing the chamber to fail. Moreover, most wall materials lose strength and become weaker as temperature is increased. Active cooling is thus essential to reduce the wall temperature to an acceptable value.

This study will focus on one of the steady state methods in use today called regenerative cooling. Regenerative cooling is achieved by circulating one of the liquid propellants (usually the fuel) in a cooling jacket around the combustion chamber before being injected into the chamber. The heat absorbed by the coolant augments the initial energy content of the propellant prior to injection. Regenerative cooling has proven to be effective in applications with high chamber pressures and high heat transfer rates.

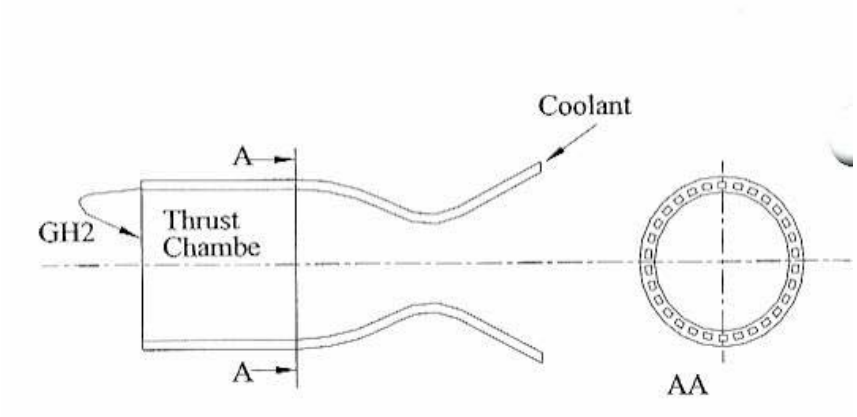

Figure 2. A typical regeneratively cooled rocket engine

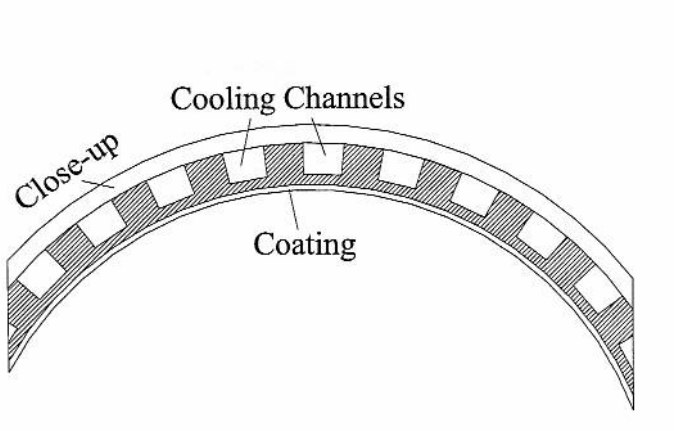

Figure 3. Detailed layout of the cooling channels in a typical regeneratively cooled rocket engine

B. FILM COOLING

Film cooling is an auxiliary cooling method applied to the chamber wall that augments regenerative cooling. It involves a relatively cool thin fluid film covering and protecting the exposed inner wall surfaces from excessive heat transfer from the hot chamber gases. In this study, the process is similar, but differs from film cooling in that extra fuel is admitted into the chamber near the wall to form a fuel layer to cover the exposed wall surface to reduce heat transfer. It does not include a chamber cooling jacket or film cooling manifolds.

Interestingly, the injection of fuel into the chamber near the wall does have a thermal insulation effect with hydrocarbon fuels. It is possible to form small carbon particles or soot near the wall. A thin, mildly adhesive soot can be a good insulator. Figure 2 shows the typical temperature distribution from the hot combustion gases to the exterior of the chamber wall.

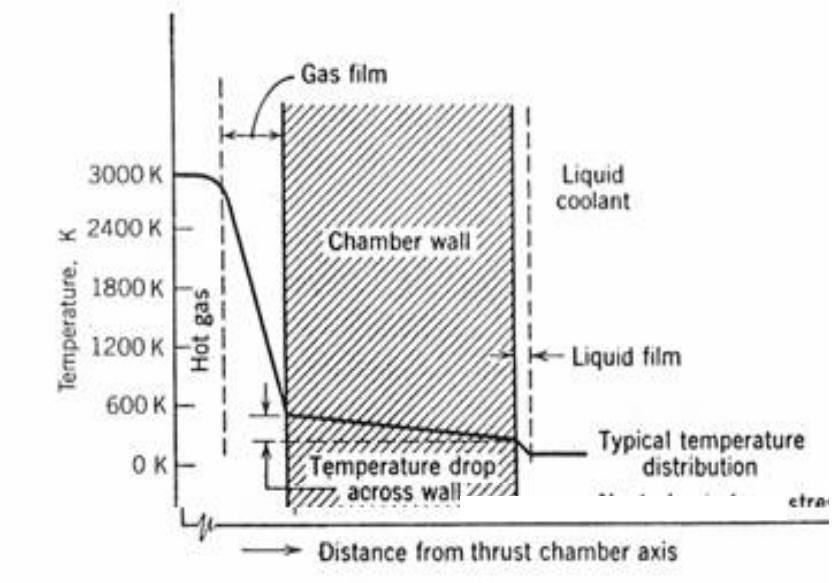

Figure 4. Typical temperature distribution of combustion chamber across wall

C. ENGINE COOLING SYSTEM CONFIGURATION

The typical liquid rocket engine employs both regenerative and film cooling, which are the primary and complementary mode of cooling for the chamber wall. The fuel is injected at the nozzle end to cool the exterior of the chamber wall (regenerative cooling), and thereafter is injected into the combustion chamber near to the wall to form a fuel layer along the wall (film cooling), as shown in Figure 5:

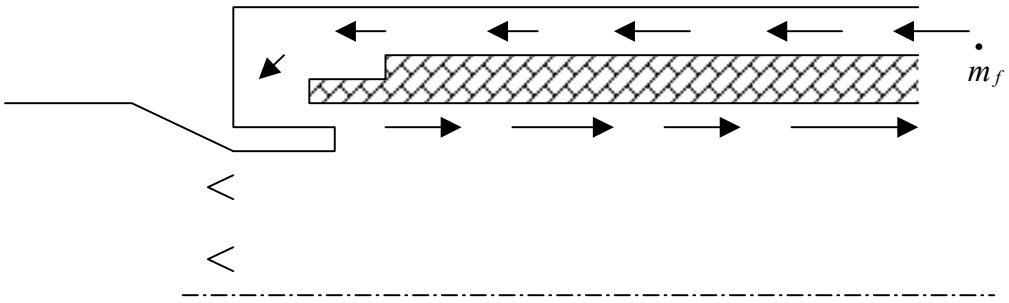

Figure 5. Engine cooling system configuration

The fuel flowing out of the fuel tank is in the range of about 300 K, when it is injected at the nozzle end to cool the exterior of the chamber wall. As it flows along the exterior of the wall, it absorbs heat, hence cooling the chamber wall. At the fuel inlet (into the chamber), the bulk temperature of the fuel is usually slightly higher than the wall temperature.

THIS PAGE INTENTIONALLY LEFT BLANK

III. NUMERICAL MODELING

A. NUMERICAL TOOLS

The key numerical tool used for this numerical study is the commercially available flow solver called CFD-ACE. The model grid is created using its grid generation module, CFD-GEOM. The simulations were done in the primary solver module, CFD-ACE, which includes modules on Flow, Heat transfer, Radiation and Turbulence. The output was viewed through its post-processor module, CFD-VIEW.

Two other numerical tools that were used to provide the necessary input parameters to CFD-ACE are the Thermo-Chemical Equilibrium Program (TEP), and RADCAL. TEP is used to calculate the properties of the combustion gases such as density, thermal conductivity, kinematic viscosity, mole fractions of the constituent combustion gases, etc. TEP is also used to calculate the properties of the fuel RP1 at different pressures and temperatures. RADCAL, originally developed by NIST, is used to determine the active spectral radiation bands of the combustion gases within the chamber.

B. NUMERICAL MODEL

The combustion chamber of the rocket engine is assumed to be a simple cylinder of diameter 1.5” (0.0381metres) and length 3” (0.0762 metres). These dimensions correspond to that of the hydrocarbon fuel film-cooled rocket engine being concurrently used in laboratory experiments at NPS.

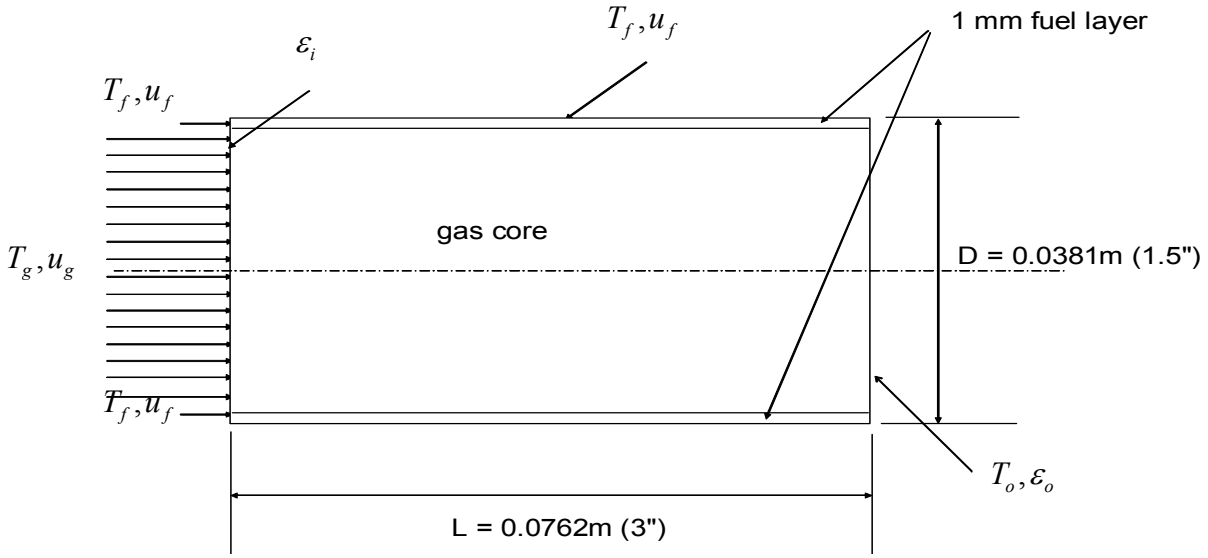

Figure 6. Detailed schematic of a scaled down model

The cylinder wall is isothermal with a constant temperature T_w and the wall has an emissivity ε_w. The combustion gas, which is participating (absorbing, emitting but non-scattering) and non-gray, enters the combustion chamber through the gas inlet into the core of the cylindrical chamber. The extra fuel (RP1) is injected through a fuel inlet near the combustion chamber walls so as to provide a uniform fuel layer on the wall.

1. Combustion Gas

The gas is assumed to enter the core of the combustion chamber at a uniform velocity of 122.5 m/s at 3500K and 35 atmospheres. A velocity of 122.5 m/s, which corresponds to a Mach number of about 0.1, will keep the study well within the incompressible regime of fluid flow.

The products of the combustion process are determined based on a typical O/F ratio of 2.3. The properties of the combustion gases such as density, thermal conductivity, and kinematic viscosity are evaluated by TEP in its rocket module. The inputs required by TEP are the reactants, namely the fuel (RP1) and the oxidizer (gaseous oxygen), the chamber pressure and temperature, and the O/F ratio. An example of the typical output from TEP is shown in Appendix A.

2. Fuel (RP1)

The fuel RP1 is injected through a fuel inlet of 1mm annular thickness adjacent to the combustion chamber wall. The fuel is injected at a uniform velocity at 500K, which is the wall temperature. The properties of RP1 at the specified temperature and chamber pressure are calculated by TEP in its gas properties module.

As actual data for RP1 for its critical temperature and pressure is unavailable, a good reference close to RP1 is kerosene.

Liquid coolant	Boiling characteristics					
	Pressure (MPa)	Pressure (Atm)	Temperature (K)	Critical Temperature (K)	Pressure (MPa)	Pressure (Atm)
Kerosene	0.101	0.997	490	678	2.0	19.738
	0.689	6.800	603			
	1.38	13.619	651			
	1.38	13.619	651			

Table 2. Heat Transfer Characteristic of Kerosene [5]

At such a high injection pressure of 35 atmospheres (twice its critical pressure (P_c)) and temperature of 500K,(though below its critical temperature (T_c) but above its boiling point) , RP1 exists as a supercritical fluid (SCF). This can be explained through a typical phase diagram in Figure 7.

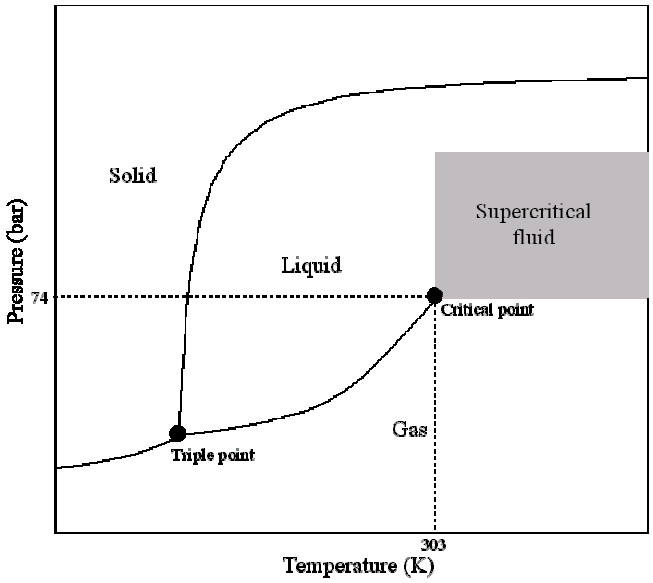

Figure 7. Typical phase diagram

The triple point is well known as the thermodynamic state at which the three phases, namely gas, liquid and solid, of a pure substance co-exist. The gas-liquid co-existence curve is known as the saturation curve. As both temperature and pressure increase along the saturation curve, the liquid becomes less dense due to thermal expansion and the gas becomes denser as pressure rises. Eventually the densities of the two phases converge and become identical; the distinction between gas and liquid disappears. Thus, a supercritical fluid is a liquid and a gas in itself when it is above its critical point. That also explains the rationale of using TEP (gas properties module) to calculate the properties of RP1 in the study.

C. RADIATION TRANSPORT

1. Gas Radiation Transport

The absorption and emission characteristics of gases depend on the thermodynamic state of the gas. In general, gases absorb and emit only in narrow wavelength bands. Gases of combustion products are known to be participative in radiative transport even at relatively low pressures and temperatures. Thus, their presence cannot be ignored and the gas should be treated as non-gray. Treating combustion gases as gray is grossly inaccurate although it is often done to obtain an approximate idea of its behavior. Hence, the combustion gas is treated as non-gray in the study.

The Discrete Ordinate Method (DOM) is employed in CFD-ACE to solve the Radiative Transport Equation (RTE). DOM is basically a tool to transform the RTE into a set of simultaneous partial differential equations. It is based on a discrete representation of the directional variation of the radiative intensity. But the absorption coefficient (κ) is needed to solve the RTE.

To obtain the absorption coefficient, the study employed the box model developed by Penner [3]. $\overline{\kappa}$ is assumed to be related to the band intensity α by

$$\overline{\kappa} = \frac{\alpha}{\Delta \eta_e} \tag{3.1}$$

The band intensity α is obtained using the Exponential Wide Band model. $\Delta \eta_e$ is obtained using the output plots of RADCAL . In other words, the spectral bands of the emission/absorption of the combustion gas within the infrared spectrum are derived from the output plots of RADCAL. The determination of the spectral bands of the combustion gas is covered in detail in Appendix B. A

typical RADCAL output file is also enclosed in Appendix B. The calculation of the absorption coefficient is covered in detail in Appendix C with a numerical example.

2. Fuel Layer Radiation Transport

As RP1, in the supercritical state, is as much a liquid as it is gas, it is treated as gray and diffuse. A key relationship between emissivity ε and the absorption coefficient κ is:

$$\varepsilon = 1 - e^{-\kappa X} \tag{3.2}$$

The optical path length is taken to be the thickness of the fuel layer since we have a thin sheet of fuel film on the wall. The effects of the absorption coefficient, and hence emissivity, of the fuel layer (different fuel properties) on the heat transfer to the wall will be further studied in the course of this study.

D. GRID GENERATION

The grid model was created as an axi-symmetric two-dimensional structured grid. There are a total of 20,900 nodal pts in the computational grid model. 100 grid points were placed on the axial edge of model. The grid points are distributed based upon a power law distribution.

$$u[n] = \left(\frac{n-1}{npts-1}\right)^{x} \tag{3.3}$$

where
- *u(n)* - location of the *nth* grid point in the interval
- *n* - grid point index on the interval
- *npts* - the total number of grid points
- *x* - user specified power

x corresponding to unity (1) will return a uniform distribution. For non-unity powers, there are forward, backward or symmetry options to indicate how the power law grid distribution should be applied.

In the axial direction, a power law exponent of 2 was applied symmetrically, such that there are more grid points at the inlet and outlet, which are the areas of focus.

For the radial direction, there are a total of 210 grid points over two edges, which defined the zones for the fuel layer and the gas core. They were named as fuel inlet/outlet (80 grid points) and gas inlet/outlet (130 grid points) respectively. The distribution in the fuel layer was set to unity (uniform distribution) and that of the gas core was set with the power law = 1.5 with more grid points towards the fuel-gas interface. The radial distribution was set as

such, so that the radial grid will be refined in a gradual manner from the centerline/symmetry line towards the interface and uniform thereafter till it reaches the wall.

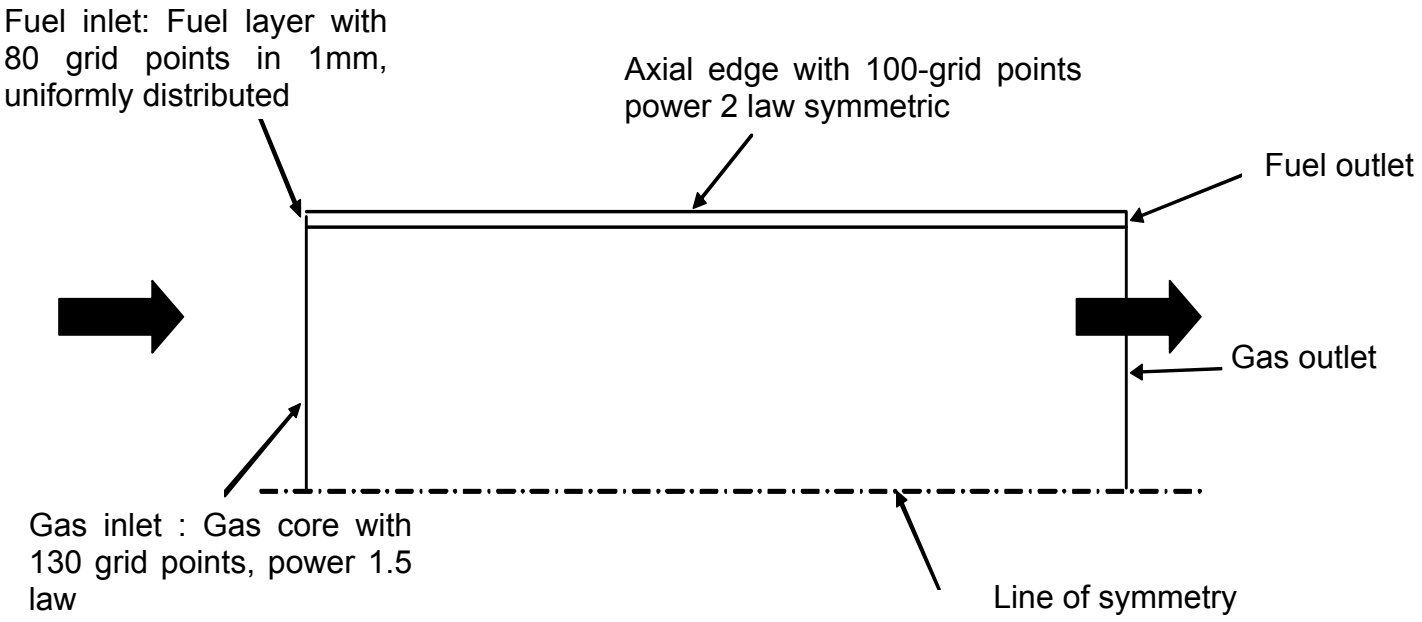

Figure 8. Grid model: Axi-symmetric 2-D grid

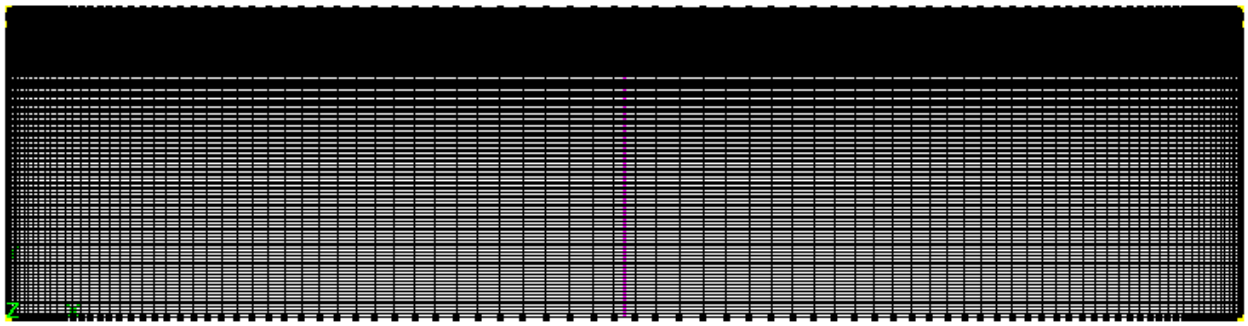

Figure 9. Grid model as in CFD-GEOM

E. TEST FOR CONVERGENCE CRITERION

The convergence criterion for maximum error between iterations was set to $1e^{-10}$. The residuals of the computational variables are checked for a reduction of 3 to 5 orders of magnitude for stability and proper convergence of the solution. In addition, the output or solution is checked for mass and energy conservation.

THIS PAGE INTENTIONALLY LEFT BLANK

IV. THEORETICAL ANALYSIS/INVESTIGATION

A. PROCESSES/INTERACTIONS

In the fundamental understanding of the model and the flow, there are some basic processes or interactions within the model.

1. Heat Transfer

In the area of heat transfer, the important modes are convection and radiation. In the model, there is convective heat transfer between the wall and the fuel layer; and between the fuel layer and the gas core. In radiation, every element radiates on account of its own temperature, hence the wall, the fuel layer and the gas core are all radiating. Due to the radiation of objects in its vicinity, an element also absorbs the radiation of other objects, depending primarily in the property of absorptivity of the element. Thus, the wall absorbs the radiation of the fuel layer and gas core. How much it absorbs from the radiation of the gas core will depend on the transmittivity, and hence the absorptivity of the fuel layer. The fuel layer absorbs the radiation of wall and gas core directly. And the gas core absorbs the radiation from the fuel layer directly and from the wall indirectly.

2. Shear Forces

In addition to heat transfer, there is also the presence of shear forces due to the different velocities of flow. A shear effect will be present at the wall due to the no-slip condition of the wall; and also at the interface of the fuel layer and gas core. At the interface, the faster gas layer tends to dragging along the slower fuel layer in its flow.

B. GOVERNING EQUATIONS/ANALYSIS

The chamber wall is isothermal at temperature T_w, the fuel layer with inlet conditions T_f and u_f, and the gas core with inlet conditions T_g and u_g.

The simplified governing equations that will help in the understanding of the interactions between the different elements are presented below:

Wall : $q_{wall} = h(T_f - T_w) - \varepsilon_w \sigma T_w^{\,4} + \alpha_w \varepsilon_f \sigma T_f^{\,4} + \alpha_w (1-\alpha_f)\varepsilon_g \sigma T_g^{\,4}$ (4.1)

where

$h(T_f - T_w)$ = convective heat transfer between the wall and the fuel

$\varepsilon_w \sigma T_w^{\,4}$ = radiative emission of the wall due to its temperature

$\alpha_w \varepsilon_f \sigma T_f^{\,4}$ = heat absorption by the wall due to the radiative emission of the fuel layer

$\alpha_w (1-\alpha_f)\varepsilon_g \sigma T_g^{\,4}$ = heat absorption of the wall due to the transmittance of the fuel of the radiative emission of the gas.

Fuel layer: $q_{fuel} = h_1(T_w - T_f) + h_2(T_g - T_f) - \varepsilon_f \sigma T_f^{\,4} + \alpha_f \varepsilon_w \sigma T_w^{\,4} + \alpha_f \varepsilon_g \sigma T_g^{\,4}$ (4.2)

Gas core: $q_{gas} = h(T_f - T_g) - \varepsilon_g \sigma T_g^{\,4} + \alpha_g \varepsilon_f \sigma T_f^{\,4} + \alpha_g (1-\alpha_f)\varepsilon_w \sigma T_w^{\,4}$ (4.3)

The conventions for the signs in the heat flux are positive (+) for wall heat gain and negative (-) for wall heat loss for each element.

C. MODEL ASSUMPTIONS

1. The combustion process between the fuel and the oxidizer is assumed to be a complete oxidation reaction. Thus, the composition of the combustion of the constituent gases is assumed “frozen”, i.e. fixed for the duration of the modeling.

2. The fuel layer injected is modeled to cover the entire inner wall of the combustion chamber along the entire length of the chamber.

3. The wall is assumed to be at a constant temperature from the inlet to the outlet. It is assumed that the regenerative cooling on the exterior of the chamber wall will be able to remove all the excess heat to keep the wall temperature constant throughout.

D. DETERMINATION OF MODEL PARAMETERS

The model parameters that were fixed in this study are the following:

Chamber pressure (atm)	35
Gas temp (K)	3500
Fuel inlet temperature (K)	500
Inlet/outlet emissivity	0

Table 3. Fixed model parameters

The chamber pressure of 35 atmospheres is typical and was specially selected for evaluation due to the experimental data available for reference. The gas temperature of 3500K and wall temperature of 500K are also typical figures

from experiments. The fuel inlet temperature is assumed to be 500K after the regenerative cooling of the exterior chamber wall as depicted in Figure 5. The inlet and outlet emissivities are set to zero due to the lack of data and accurate methods to determine them.

E. PARAMETRIC STUDIES

1. Varying Absorptivities For Fuel RP1

The radiation properties for RP1 are not available in the open sources. In the study, the fuel layer is assumed to be gray and diffuse, hence its emissivity and absorptivity are equal. For the study, the absorptivity was varied from 0.3 (which is optically thin) to 0.9 (optically thick, as that of soot).

Using equation (3.2)

$$\varepsilon = \alpha = 1 - e^{-\kappa X} \tag{3.2}$$

The absorption coefficient of RP1 based on the different absorptivities can be calculated as follows:

Absorptivity (α)	Absorption coefficient (κ, m^{-1})
0.3	356
0.5	694
0.7	1205
0.9	2303

Table 4. Absorptivities and absorption coefficients for RP1

2. Varying Film Cooling Ratios

The film-cooling ratio is defined as the ratio of the mass flow rates of the fuel film to that of the core gas flow as follows:

$$\beta = \frac{\dot{m}_{fuel}}{\dot{m}_{gas}} \tag{4.4}$$

With the fuel inlet fixed,

$$\beta = \frac{\dot{m}_{fuel}}{\dot{m}_{gas}} = \frac{\rho_f A_f u_f}{\rho_g A_g u_g} \tag{4.5}$$

At the given inlet pressure and temperature, the densities of the fuel and gas remain constant. The cross-sectional areas for the fuel and gas inlet are fixed too. The varying parameter will be the fuel inlet velocity v_f and gas inlet velocity v_g .

According to mixing theory, the intensity of the mixing at the fuel-gas interface is dependent on the absolute velocity difference of the adjacent layers Δu , i.e. $u_g - u_f$. Thus the new gas velocity for a new inlet fuel velocity will be:

new u_g = new $u_f + \Delta u$ (4.6)

u_f (m/s)	u_g (m/s)	Film cooling ratio β	Remarks
30	122.5	**25.3%**	$\Delta u = 92.5$ m/s
22	114.5	**19.8%**	$\Delta u = 92.5$ m/s
15	107.5	**14.4%**	$\Delta u = 92.5$ m/s

3. Varying Wall Temperatures

The wall temperature is assumed to be constant, and a parametric study was conducted for values of 500K, 700K and 900 K.

V. RESULTS AND DISCUSSION

A. TYPICAL VELOCITY AND TEMPERATURE PROFILES

The 2-D radial velocity profiles are shown in Figure 10 for the inlet and outlet of the combustion chamber. Figure 10 also shows the magnified velocity within the 1mm fuel layer near the wall. The absorptivity of the fuel is set to 0.3, i.e. that of the baseline model.

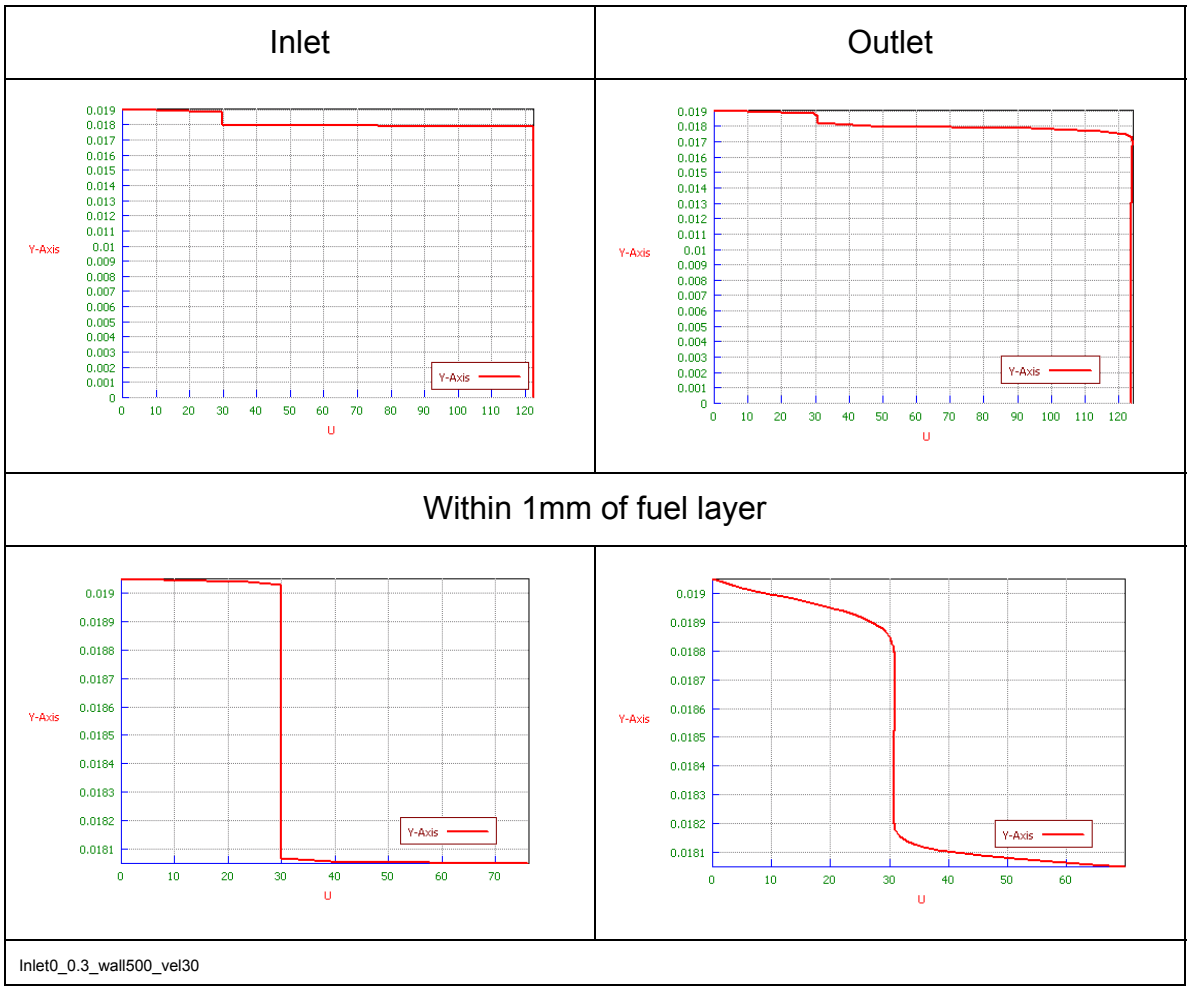

Figure 10. 2-D radial velocity profiles at the inlet and outlet

The plots show that at the inlet, the fuel comes in at a velocity of 30m/s, as compared to the gas flow at 122.5 m/s. At the outlet, it can be observed that the velocity profile has developed at the region near the wall (no slip condition), and

at the interface where the disparity between the fuel and gas velocities resulted in the faster gas core dragging along the slower fuel sub-layers.

The 2-D radial temperature profiles for the combustion chamber at the inlet and outlet are shown in the similar manner in Figure 11.

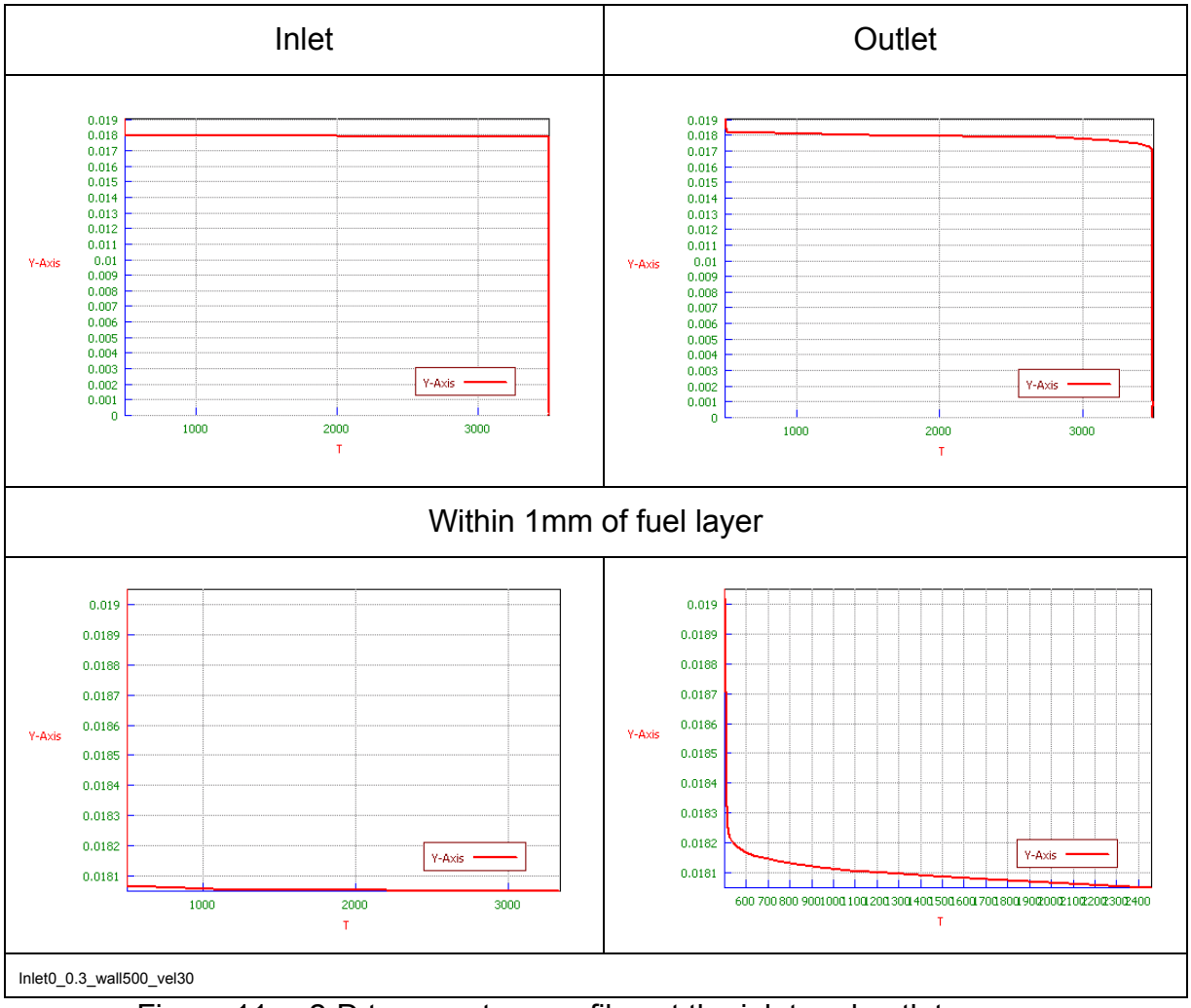

Figure 11. 2-D temperature profiles at the inlet and outlet

At the inlet, the fuel layer is at 500K and the gas core is at 3500K. At the outlet, it is shown that the temperature profile has developed at the interface. The figures show that, at the interface, the hotter gas sub layers heat up the cooler fuel sub layers. The heat interactions at interface occurs primarily though convection and radiation. Conduction effects are negligible due to the velocity

disparity of the gas and fuel layers. The wall temperature is the same as the fuel inlet temperature of 500K.

When the wall temperature is higher than the fuel inlet temperature, the typical temperature profiles are shown below:

Inlet	Outlet
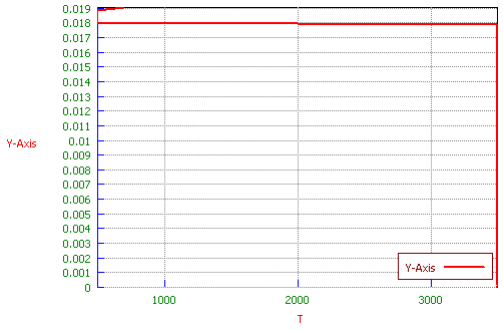	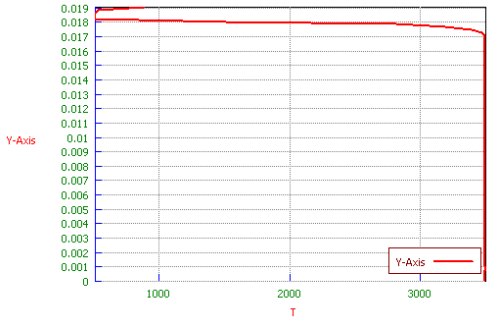
Within 1mm of fuel layer	
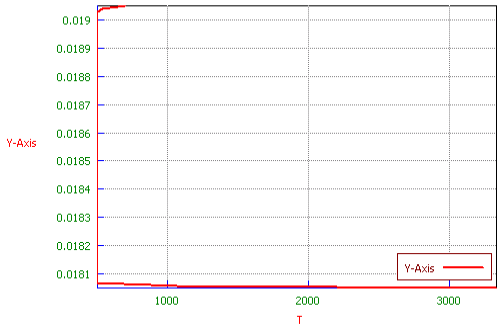	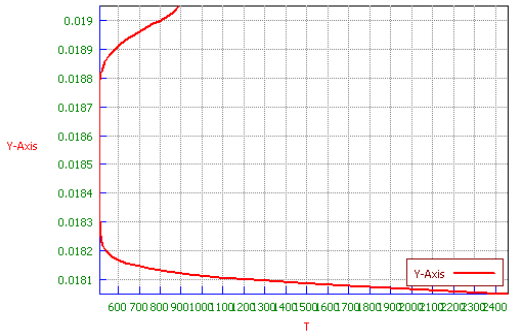
Inlet0_0.3_wall900_vel30	

The wall temperature is at 900K. The fuel layer near the wall is now being heated up by the wall (at a higher temperature), and hence the development of the temperature profile near the wall. The velocity profiles remain unchanged for a higher wall temperature.

B. BULK MEAN TEMPERATURE OF FUEL FILM

As the velocity and temperature profile within the fuel film varies from the wall to the interface, it is useful to determine the bulk mean temperature for the fuel film from its definition below:

$$T_{bulk} = \frac{1}{U_m A_C} \int (T \times u) dA_c \qquad (5.1)$$

By 2D approximation, the formula is modified to

$$T_{bulk} = \frac{1}{U_m y} \sum T_i \cdot u_i \triangle y \qquad (5.2)$$

where y = 1mm, the approximate thickness of the fuel film.

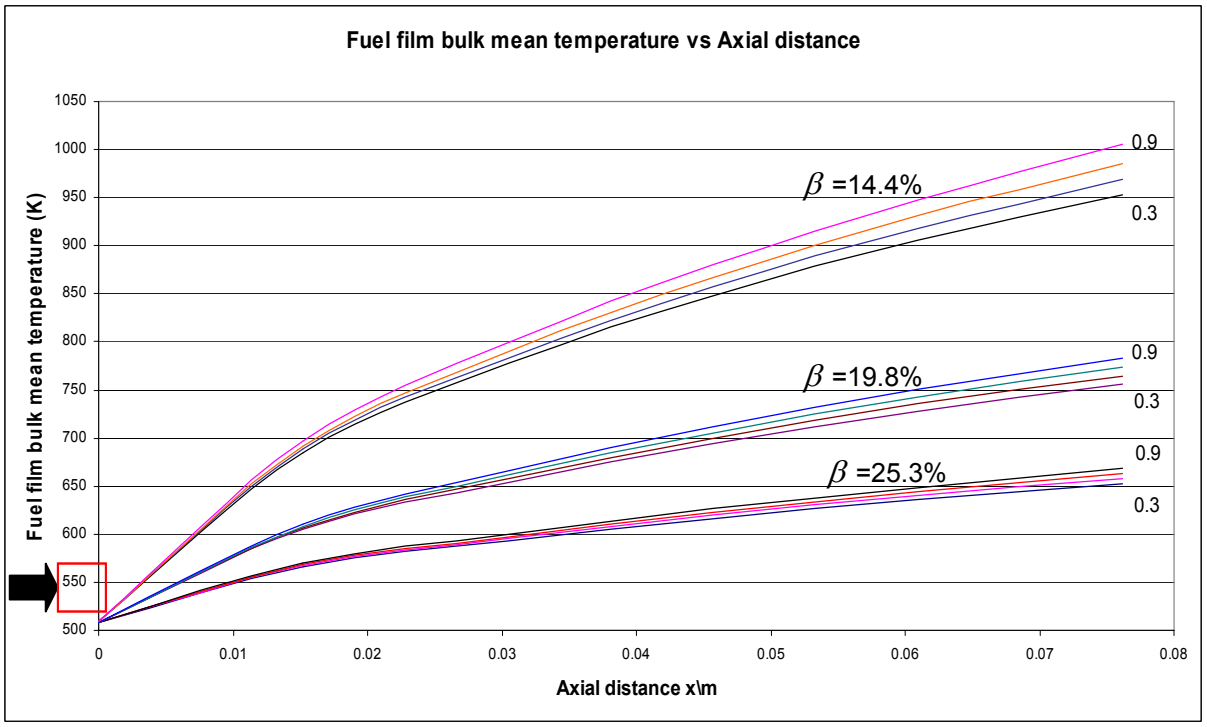

Figure 12. Typical fuel film bulk mean temperature plot

Figure 12 shows a typical fuel film bulk mean temperature plot for different absorptivities (α =0.3, 0.5, 0.7 and 0.9) of the fuel film. The increase in the fuel film bulk mean temperature from the inlet to the outlet is dependent on the fuel absorptivity α and film-cooling ratio (β).

An optically thin ΔT_{bulk} ($\alpha = 0.3$) fuel film absorbs less of the radiation from the gases, allowing more to pass through it to the wall. Thus, the increase in the bulk mean temperature ΔT_{bulk} will be less as compared to an optically thick ($\alpha = 0.9$) fuel film.

A lower fuel inlet velocity translates into less fuel mass flow into the chamber near the wall, based on $\dot{m}_{fuel} = \rho_f A_f u_f$, hence a lower film cooling ratio β. Since the dynamics in the gas core is unchanged, the amount of heat flux into the fuel film remains constant. Thus with less fuel mass flow, the bulk mean temperature of the fuel film will have to increase, hence a higher ΔT_{bulk} for a lower fuel inlet velocity.

1. Significance Of The Fuel Film Bulk Mean Temperature

The increase and the rate of increase in the bulk mean temperature of the fuel film is important because it affects the total heat flux to the wall. From equation (4.1):

$$q_{wall} = h(T_f - T_w) - \varepsilon_w \sigma T_w^{\,4} + \alpha_w \varepsilon_f \sigma T_f^{\,4} + \alpha_w (1 - \alpha_f) \varepsilon_g \sigma T_g^{\,4}$$

The fuel film bulk mean temperature occurs in the first term for convective flux and the third term for radiative heat flux to the wall. A high T_f has a very significant impact in the radiative heat flux to the wall when it is raised to the fourth power.

2. Coking Of RP1 At 550K

Using the fuel film bulk mean temperature, the location of the formation of soot within the chamber near the wall can be approximated. This will assist

greatly in the experimental work where optimal sensor locations can be determined for data collection.

From Figure 12, it can be observed that RP1 will coke earlier along the axial length of the combustion chamber for a fuel film of high absorptivity or at a lower film-cooling ratio. With the inlet fuel temperature of 500K, the effect of the absorptivity of the fuel on the location of the formation of soot (x@550K) is almost negligible. However, the film-cooling ratio does have a very significant impact on where the soot will form, as shown in Figure 13.

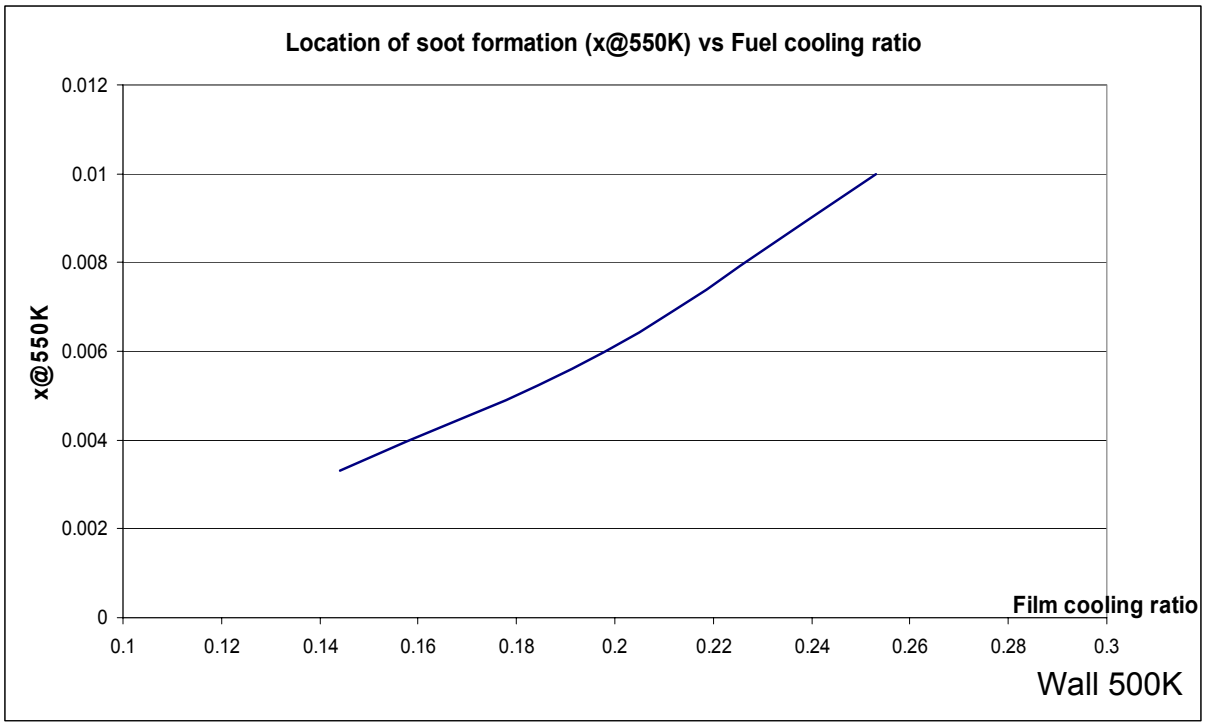

Figure 13. Location of soot formation (x@550K) vs film cooling ratio

The coking of RP1 (into soot) will translate into an almost instantaneous increase in its absorptivity α to about 0.9~1. Thus thereafter, the total wall heat flux profile will follow the curve for $\alpha = 0.9$.

C. COMPARISON OF GAS MODEL AND FUEL-GAS MODEL

1. Wall Heat Flux

The fuel-gas model is compared with the gas model to understand the effect of the fuel film on the heat transfer to the chamber wall. The common parameters between the two models are a wall temperature of 500K and the gas core of 3500K entering at 122.5 m/s.

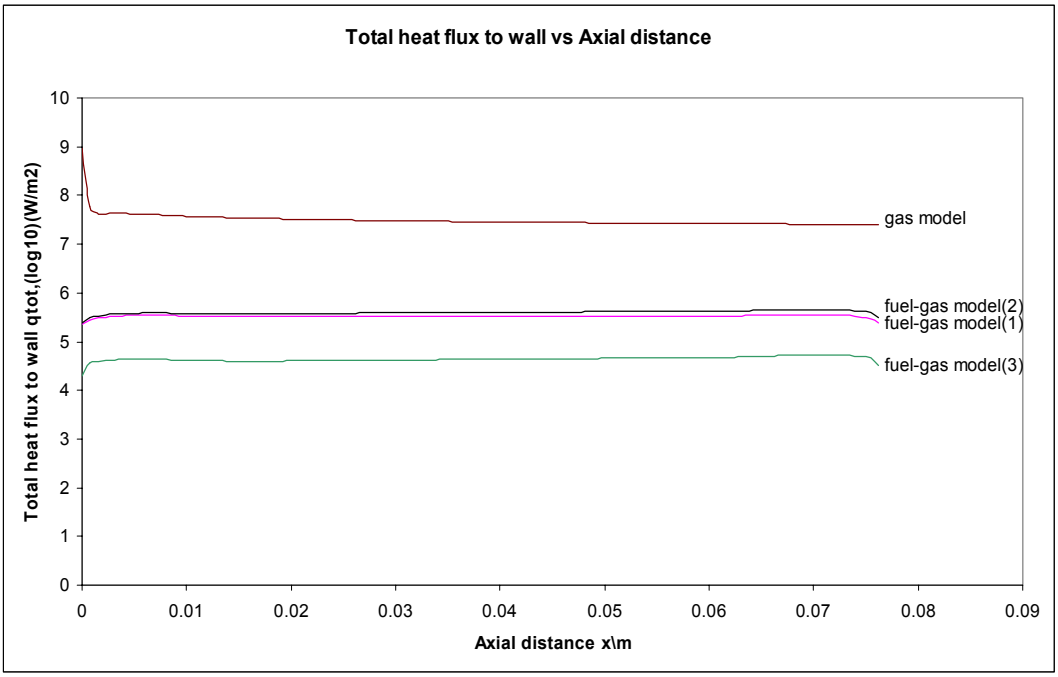

Figure 14. Comparison of heat flux to the wall for the 2 models

	Fuel absorptivity	Film cooling ratio (%)
Fuel-gas model (1)	0.3	25.3
Fuel-gas model (2)	0.3	14.4
Fuel-gas model (3)	0.9	25.3

Table 5. Parameters for fuel-gas models

The reduction of heat flux to the wall with the fuel film is very much dependent on the absorptivity of the fuel film. For optically thick (α=0.9) fuel

film, the reduction can be as much as 3 orders of magnitudes lower as in fuel-gas model (3). For optically thin (α =0.3) fuel film, the reduction is at least 2 orders of magnitudes lower (fuel-gas model (2) and (1)). This result clearly verifies the effectiveness of film cooling in reducing the heat flux to the chamber wall.

2. Dominant Mode of Heat Transfer

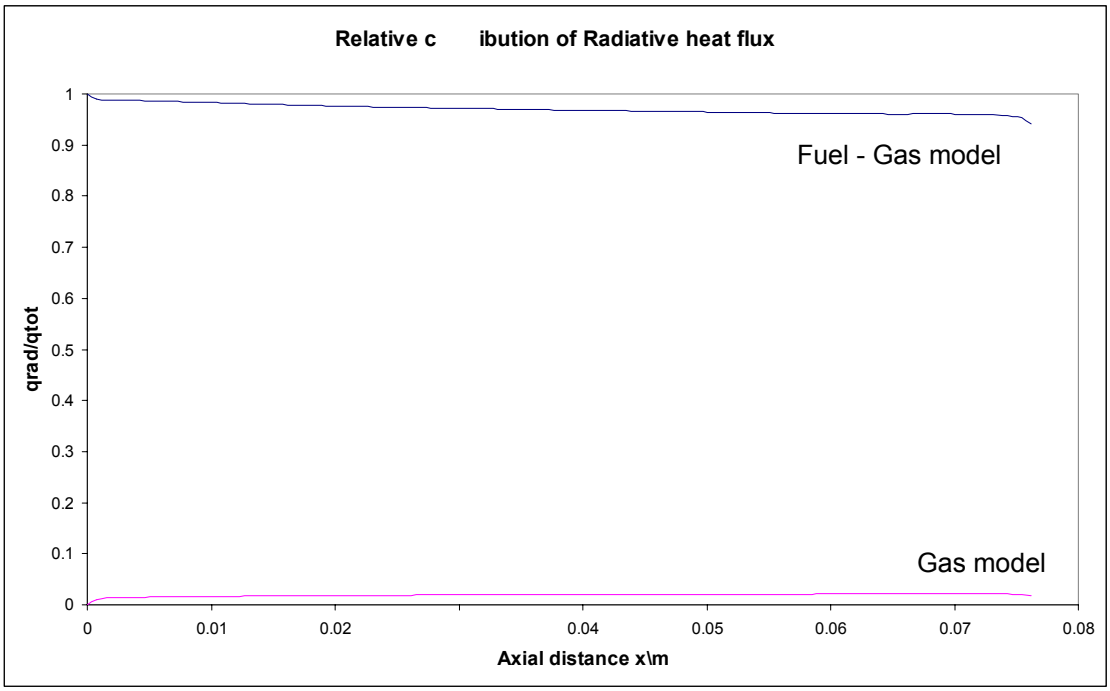

Figure 15. Relative contribution of radiation to wall heat flux for both models.

In the gas model, the dominant mode of heat transfer is convection, as the relative contribution of radiation to the wall heat flux is almost negligible. However, in the fuel-gas model, in contrast, radiation is the dominant mode of heat transfer to the wall as shown in Figure 15.

The governing wall heat transfer equation is:

$$q_{wall} = h(T_g - T_w) - \varepsilon_w \sigma T_w^{\,4} + \alpha_w \varepsilon_g \sigma T_g^{\,4} \qquad (5.3)$$

In the gas model, the convective heat transfer coefficient was much larger as the result of the large velocity and temperature differentials between the gas and the

wall. Comparatively, the heat transfer coefficient in the fuel gas model between the wall and the fuel layer is much smaller as the velocity and temperature differentials between them were much reduced.

Hence, it is important to note that the introduction of the fuel film between the wall and the gas reduces the velocity and temperature differentials between the wall and its adjacent layer (fuel film), hence the convective heat transfer coefficient and the convective heat transfer to the wall. Thus, radiation is observed to be the dominant mode of heat transfer to the wall. Conversely, increasing the velocity and temperature differentials between the wall and the fuel will increase the convective heat transfer effect to the wall. This is illustrated in Figure 15, as x increases, the fuel bulk mean temperature increases, hence increasing the temperature differential and therefore convective flux to the wall, thus the proportion of radiative flux decreases as x increases.

D. VARYING ABSORPTIVITIES FOR RP1 FUEL

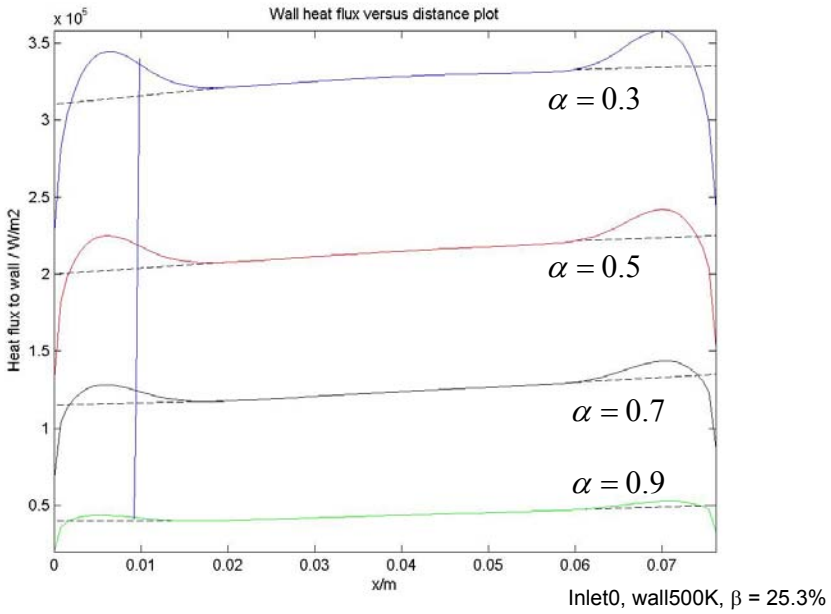

Figure 16. Heat flux to wall for varying fuel absorptivities

Figure 16 shows a typical plot for total wall heat flux to the chamber wall versus axial distance along the combustion chamber, with the wall at 500K. The almost vertical line at around x = 0.01m shows the location of the coking of RP1 where $T_{bulk} = 550K$. To the right of that line, the total wall heat flux profile should follow that of $\alpha = 0.9$ (independent of its entrance value). The twin peaks near the inlet and outlet are attributed to the artifact of numerical modeling. A more accurate heat flux profile is obtained through extrapolation from the central portion of the chamber to the inlet and outlet, as shown by the dotted lines.

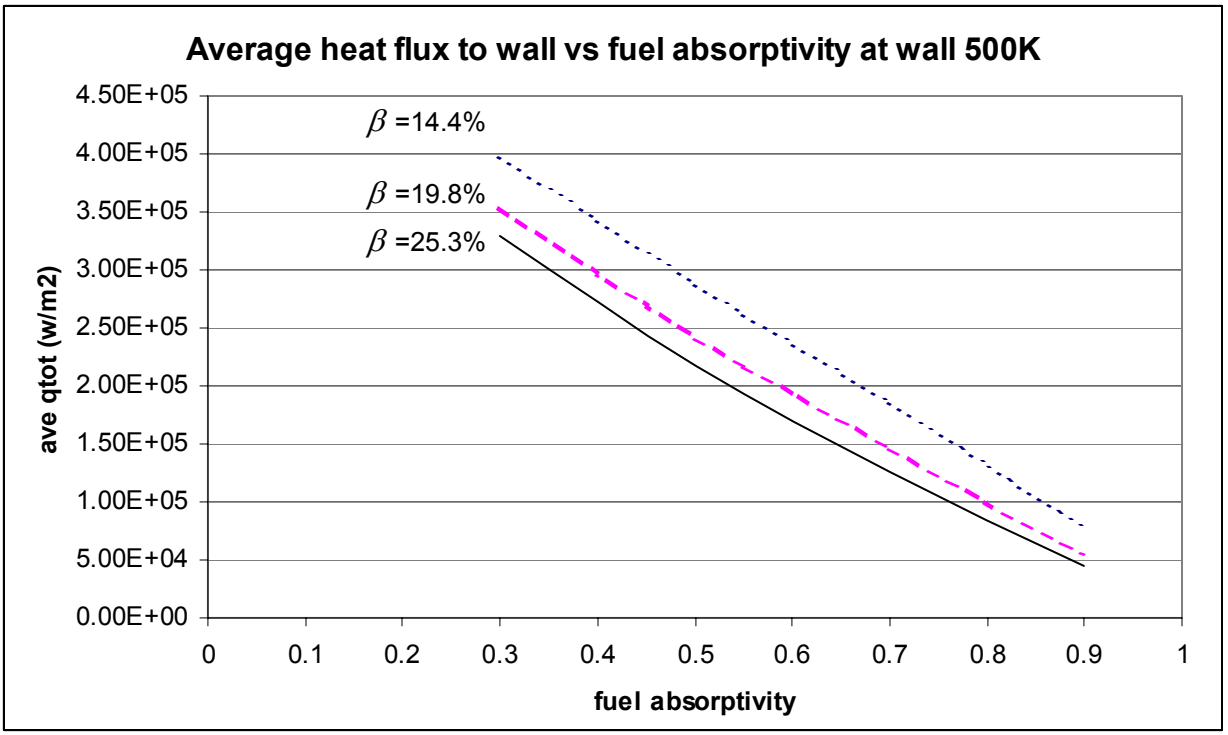

Figure 17. Average heat flux to wall vs fuel absorptivity at wall 500K

From figure 17, it can be observed that as fuel absorptivity increases, the average heat flux to the wall decreases, regardless of the film cooling ratios. This is because a fuel film of low absorptivity ($\alpha = 0.3$) allows more radiation from the hot gas core to be transmitted through, and hence a higher total heat flux absorbed by the chamber wall. Mathematically, it can be explained using equation (4.1),

$$q_{wall} = h(T_f - T_w) - \varepsilon_w \sigma T_w^{\,4} + \alpha_w \varepsilon_f \sigma T_f^{\,4} + \alpha_w (1-\alpha_f)\varepsilon_g \sigma T_g^{\,4}$$

The absorptivity α_f occurs only in the fourth term. A higher α_f will result in a lower q_{wall}, and vice versa. This finding presents the advantage of using a fuel of high absorptivity for film cooling. Alternatively, it endorses the possibility of using additives or any other means to increase the absorptivity of the fuel, so as to minimize heat flux to the wall.

E. VARYING FILM COOLING RATIO/FUEL INLET VELOCITY

As described in section B of this chapter, a lower film cooling ratio will result in a larger ΔT_{bulk}, which means a larger rate of increase of the fuel bulk temperature per unit length, and hence a higher fuel bulk temperature at each location. Reference equation (4.1), a higher T_f (in first and third term) translates to a higher q_{wall}. This is shown as in Figure 18 below:

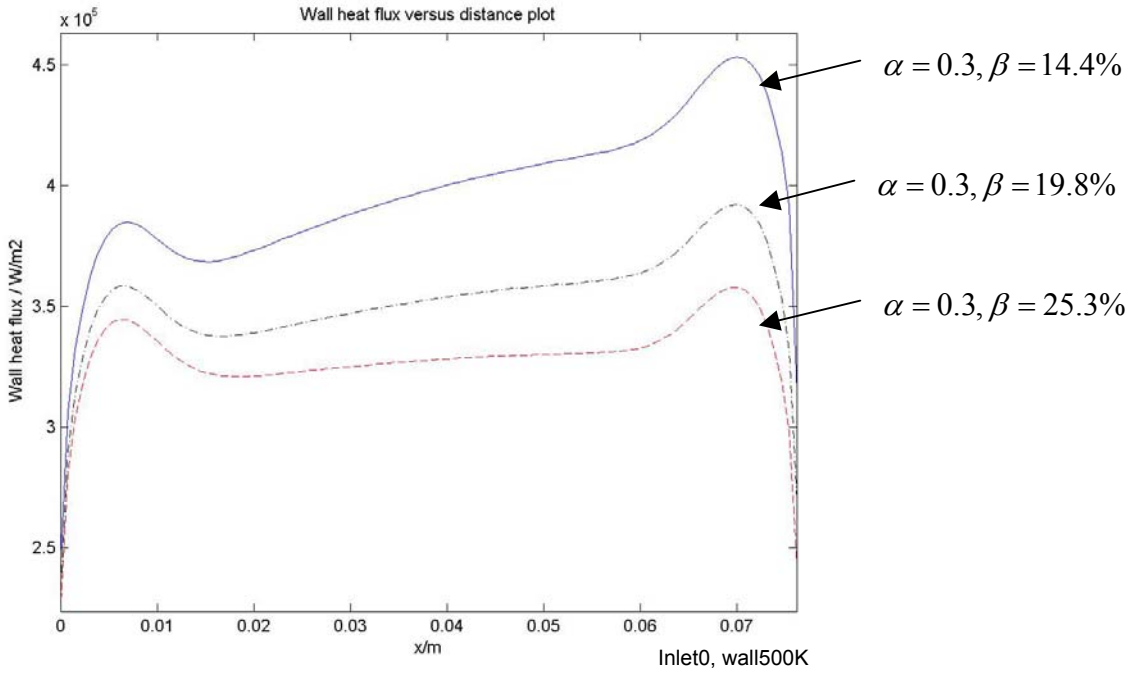

Figure 18. Heat flux plot for varying film cooling ratios

It is evident that the heat flux to the wall is increasing along the length of the combustion chamber. The rate of increase in heat flux for the different film cooling ratios is proportional to the rate of increase of the fuel bulk mean temperature as shown in Figure 19:

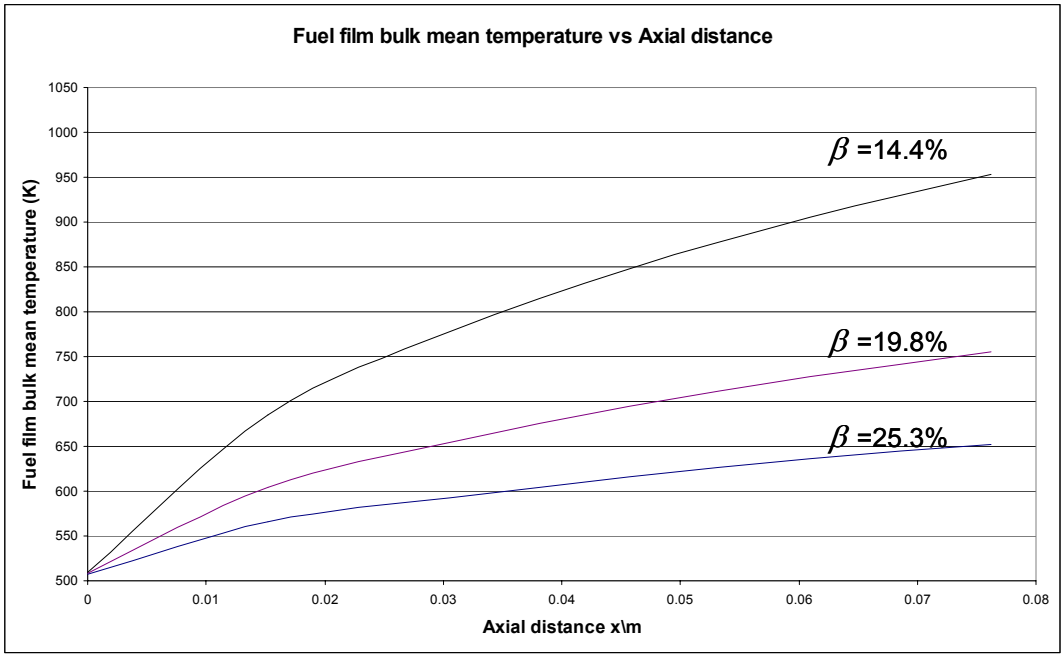

Figure 19. Fuel bulk mean temperature for different film cooling ratios

This can be inferred by referring to equation (4.1):

$$q_{wall} = h(T_f - T_w) - \varepsilon_w \sigma T_w^{\,4} + \alpha_w \varepsilon_f \sigma T_f^{\,4} + \alpha_w (1-\alpha_f)\varepsilon_g \sigma T_g^{\,4}$$

Differentiating with respect to x:

$$\frac{dq_{wall}}{dx} = h\frac{dT_f}{dx} + T_f \frac{dh}{dx} + 4\alpha_w \varepsilon_f \sigma T_f^{\,3} \frac{dT_f}{dx} \qquad (5.3)$$

Hence, with a lower film cooling ratio, $\frac{dT_f}{dx}$ is larger, and therefore $\frac{dq_{wall}}{dx}$ is larger.

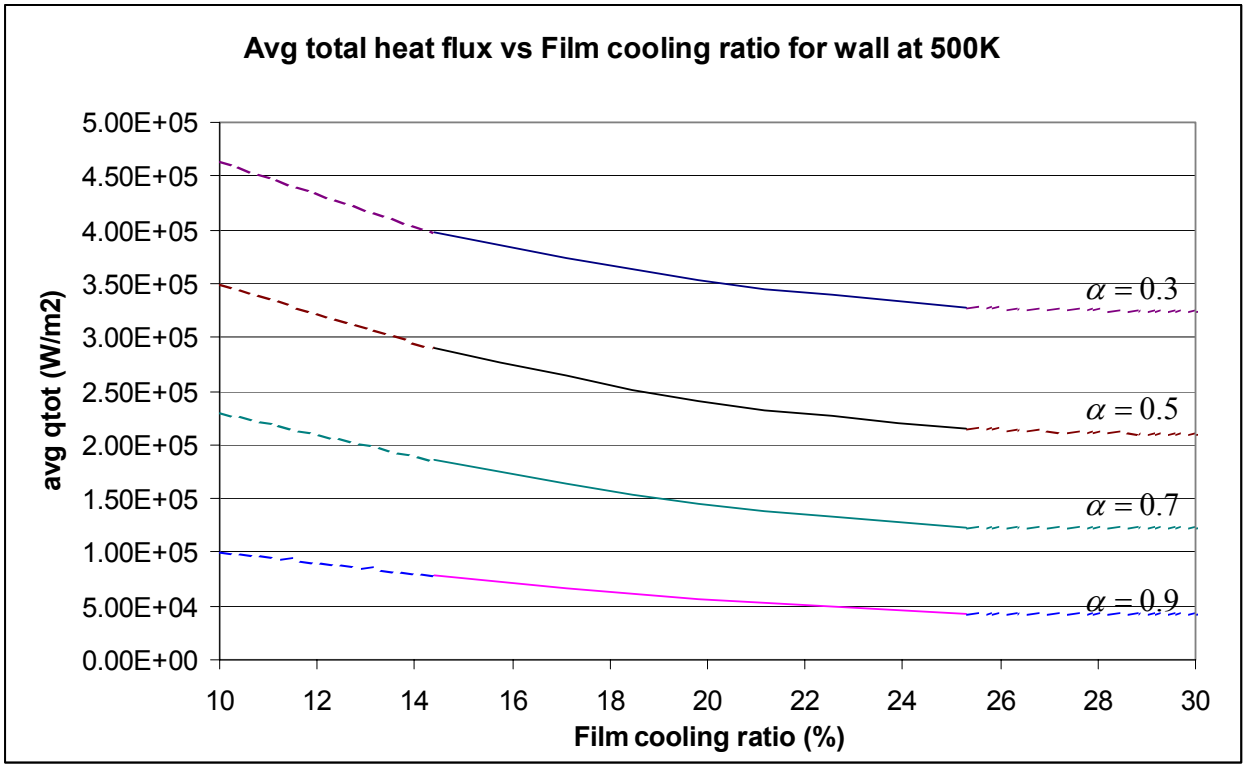

Figure 20. Average total heat flux vs film cooling ratios for wall at 500K

The average total heat flux to the wall is plotted against the different film cooling ratios in Figure 20 for different fuel absorptivities. The curves are extrapolated in both directions to 10% and 30% film cooling ratios using dotted lines. From the figure it can be concluded that with a fuel of high absorptivity (e.g. $\alpha = 0.9$), heat flux to the wall is minimized and changes in the film cooling ratios does not affect the heat flux to the wall very significantly. This finding increases the attractiveness of using a fuel of high absorptivity for film cooling, or using additives or other means to increase the absorptivity of the fuel, to minimize heat flux to the wall and also the amount of fuel required for film cooling. Secondly, it is shown that any film-cooling ratio beyond 30% has little further utility in reducing the amount of heat flux to the wall, regardless of fuel absorptivity.

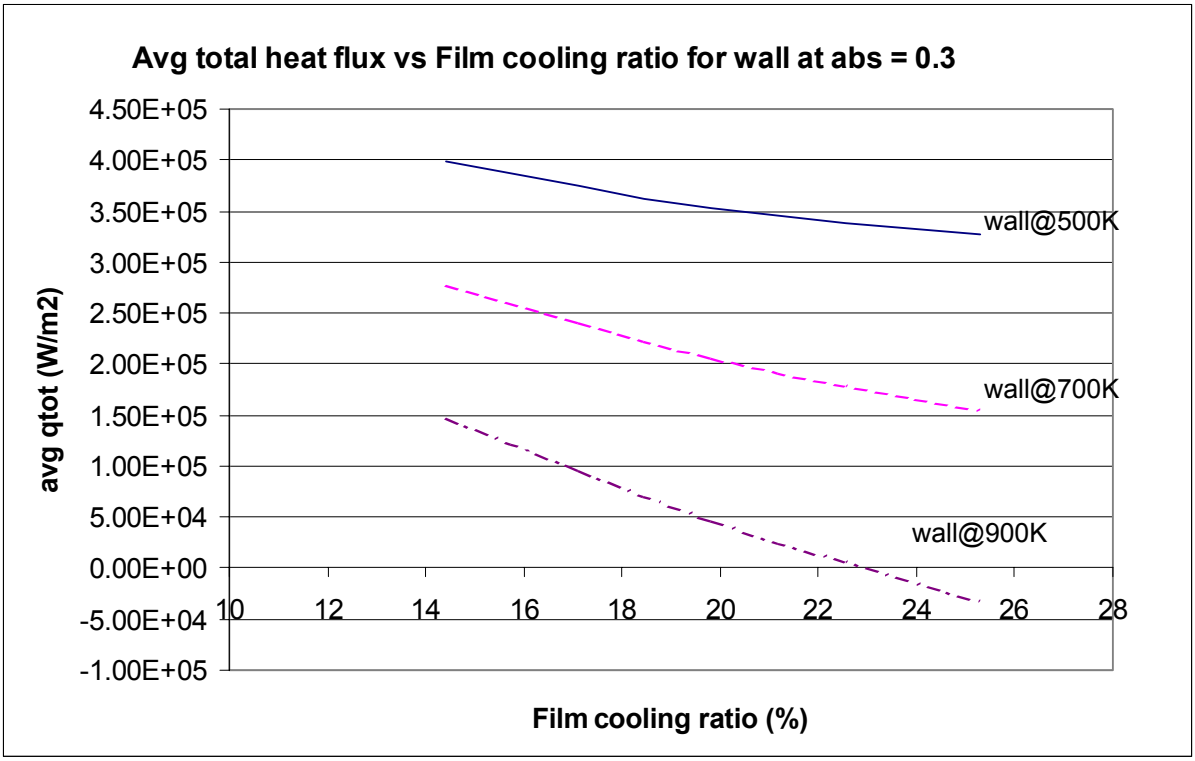

Figure 21. Average total heat flux vs film cooling ratios for different wall temperatures

Figure 21 shows the relationship between the average heat flux to the wall and the film cooling ratios for different wall temperatures. The fuel inlet temperature was set at 500K. The wall temperature is always set equal or higher than the fuel inlet temperature, as it is illogical to inject a hotter fuel film for convective cooling purposes. It is shown here that increasing the relative difference (ΔT) between the wall temperature and fuel inlet temperature helps to reduce the amount of heat flux to the wall. Thus, the desired inner wall temperature to be maintained should be determined based on safety and engineering judgment. Trying to maintain the inner wall temperature at too low a wall temperature will result in higher heat flux to the wall, and hence an increase in the overall temperature of the entire wall material.

The results had shown that maintaining an inner wall temperature of 700-800K could be optimal, as it lowers the amount of heat flux to the wall, and it offers a safety factor of about 1.5 to 2 for failure of the chamber wall material.

F. VARYING WALL TEMPERATURES

When the fuel inlet temperature is equal to the wall temperature, both convective and radiative fluxes are positive, i.e. heat is absorbed by the wall. Referring to equation (4.1):

$$q_{wall} = h(T_f - T_w) - \varepsilon_w \sigma T_w^{\,4} + \alpha_w \varepsilon_f \sigma T_f^{\,4} + \alpha_w (1-\alpha_f)\varepsilon_g \sigma T_g^{\,4}$$

For $T_f > T_w$, the third term $\alpha_w \varepsilon_f \sigma T_f^{\,4}$ will effectively negate the second term $\varepsilon_w \sigma T_w^{\,4}$, and hence the total heat flux to the wall is positive.

However, when $T_w > T_f$, the convective flux [$h(T_f - T_w)$] now becomes negative, i.e. there is a heat loss from the wall. The radiative emission, $\varepsilon_w \sigma T_w^{\,4}$, by virtue of the temperature of the wall will also have a significant effect, and will negate the effect of radiation from the fuel (third term). The overall effect of the total heat flux to the wall will then be critically dependent on the absorptivity of the fuel α_f.

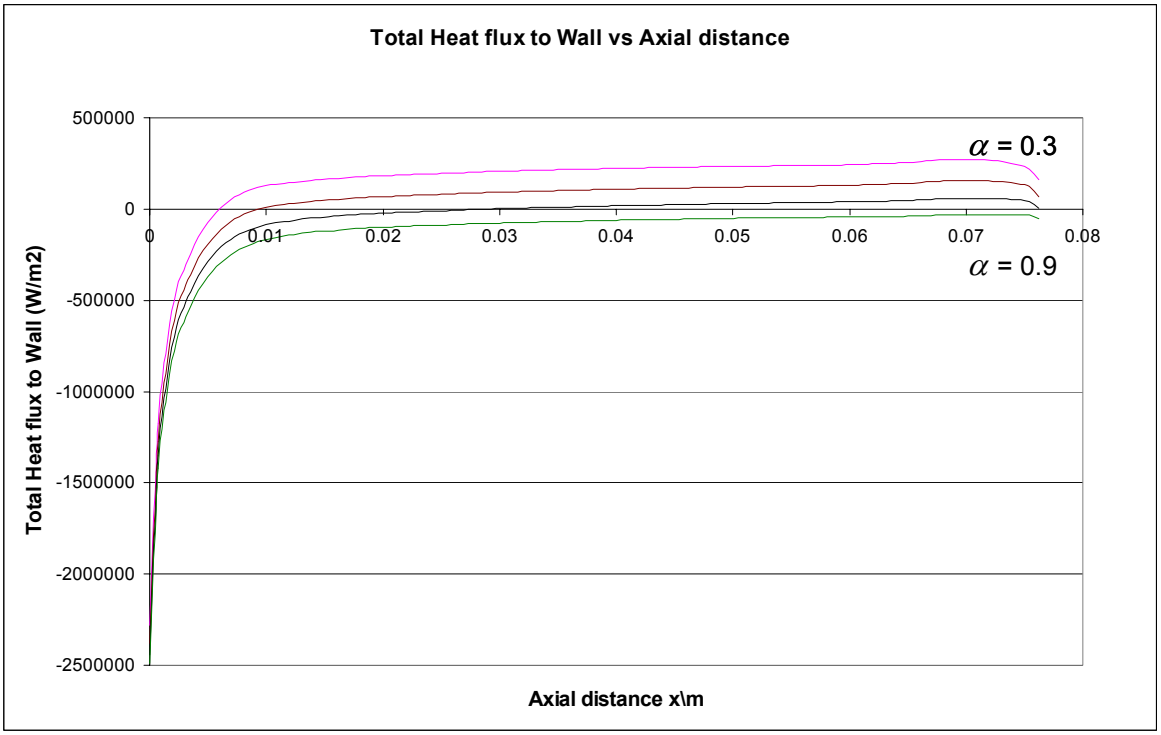

Figure 22. Total heat flux plot for wall at 700K

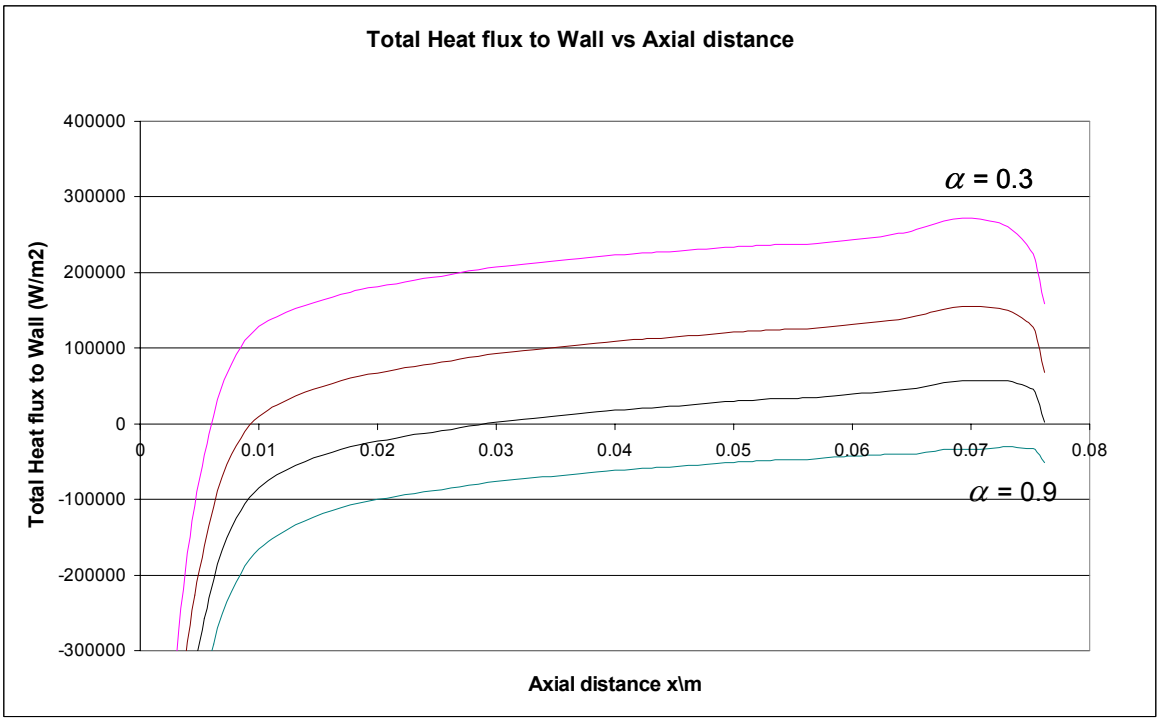

Figure 23. Total heat flux for wall at 700K (expanded)

The convective flux, which is negative, is plotted against the axial distance as shown in Figure 24.

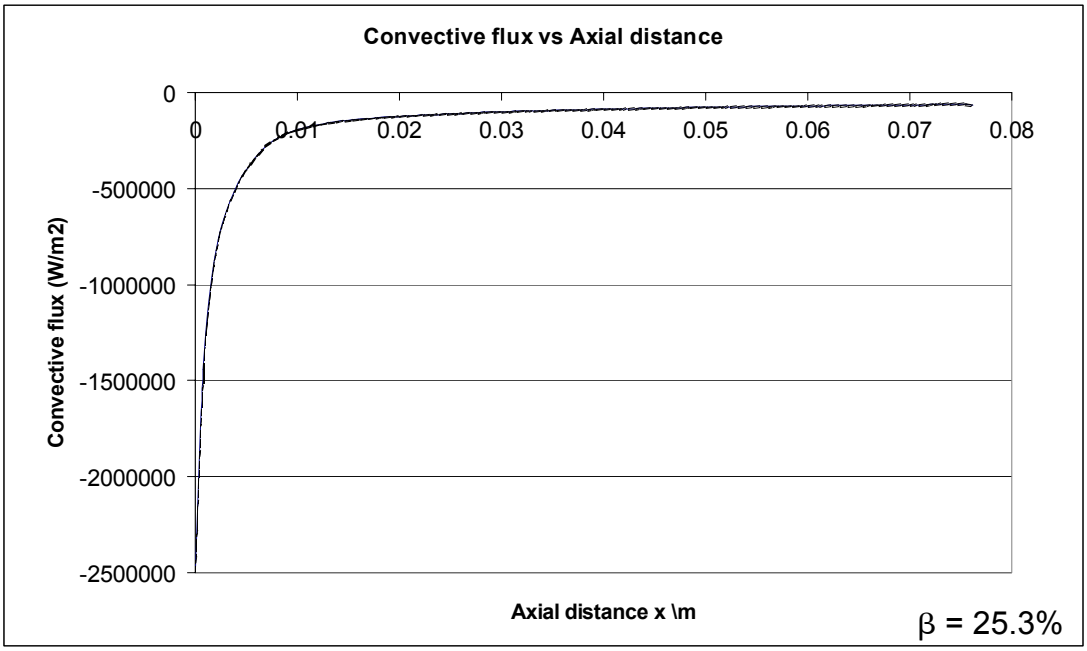

Figure 24. Convective heat flux for wall at 700K

It is important to note that the convective heat flux is not dependent on the absorptivity of the fuel α_f since

$$q_{conv} = h(T_f - T_w) \tag{5.4}$$

The plot for the radiative heat flux is shown in Figure 25.

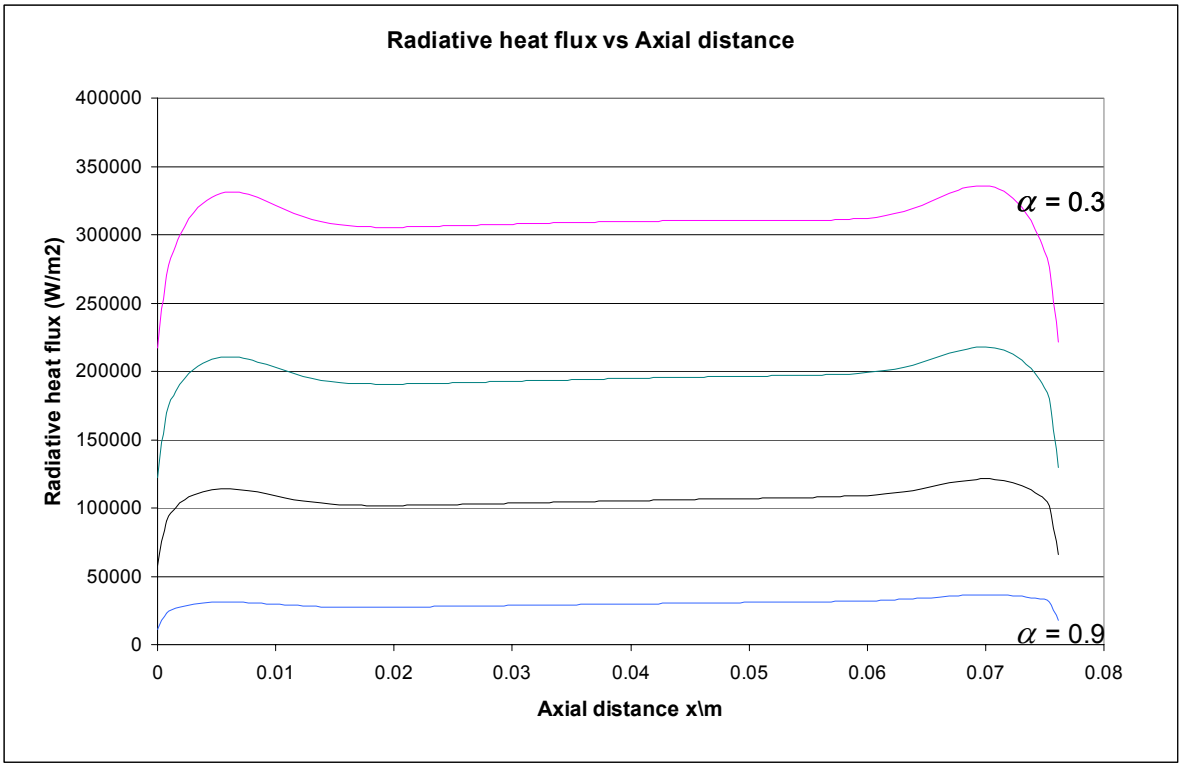

Figure 25. Radiative heat flux for wall at 700K

Superimposing the two plots on the same axes:

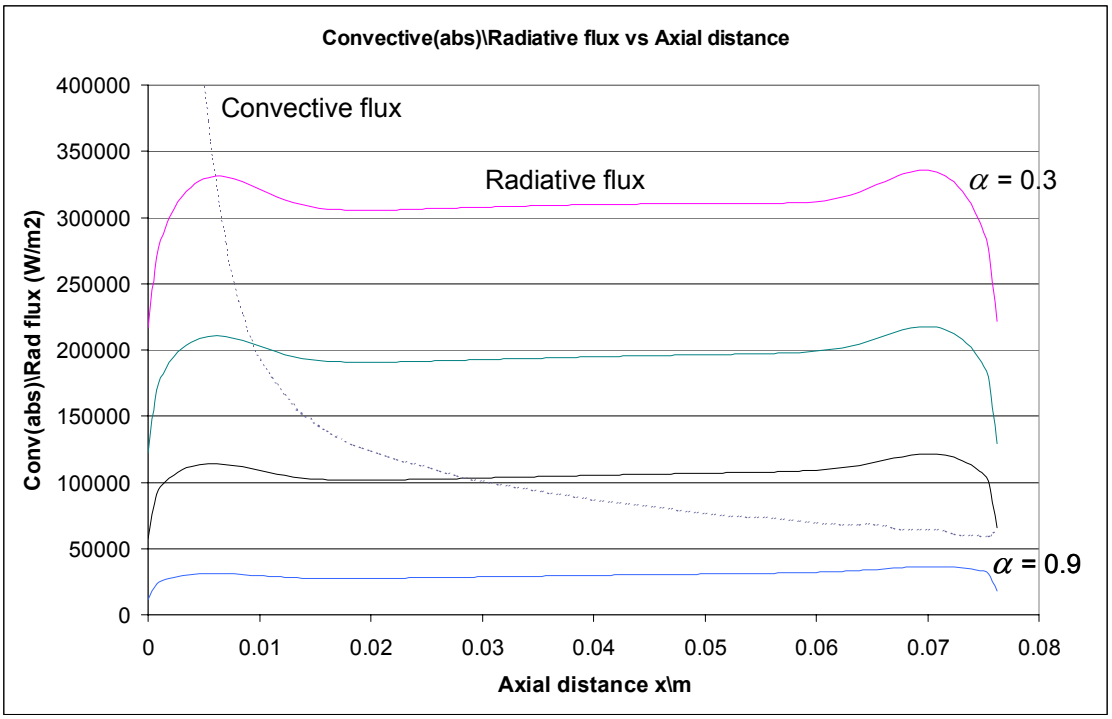

Figure 26. Superposition of convective and radiative fluxes

Comparing with Figure 23, the total heat flux to the wall equals zero where the convective flux plot intersects the radiative flux plot, i.e. where they are equal in magnitude, but opposite in sign.

Figure 26 also shows the dominant modes of heat transfer along the length of the chamber and the proportion between the two modes of heat transfer. Convection dominates in the initial length of the chamber, with $T_w > T_f$. As the axial length x increases, the fuel bulk mean temperature increases, and this reduces the convective heat flux and increases the radiative heat flux. Radiative flux dominates after the intersection point of the two fluxes. The proportion of total heat flux to the wall, where radiative flux dominates, is dependent on the absorptivity of the fuel α_f. The proportion is greater for

optically thin fuel (α_f=0.3), and decreases as the absorptivity of the fuel increases.

It is observed that the convective flux curve never intersects the radiative flux for the case of α=0.9, but is above it for the entire chamber length. This shows that the convective heat flux is greater than the radiative heat flux for the entire length, resulting in an overall heat loss by the wall to the fuel (total heat flux to wall is negative).

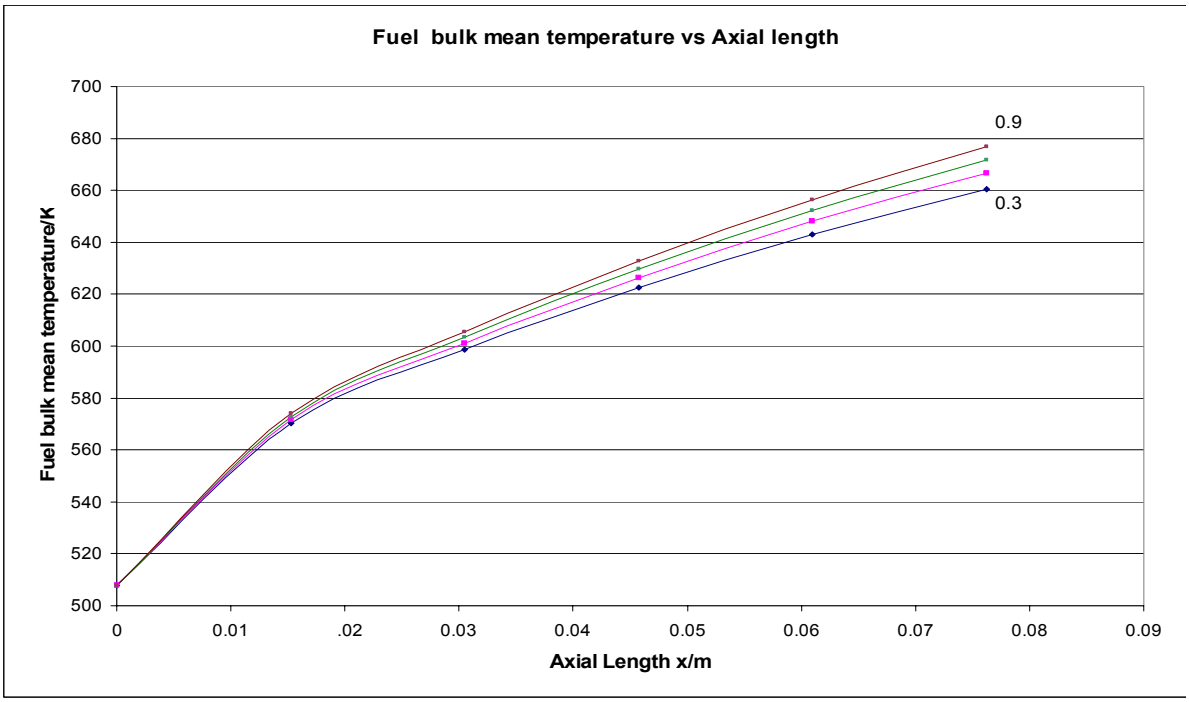

Figure 27. Fuel bulk mean temperature for wall at 700K, α=0.9

With reference to equation (4.1)

$$q_{wall} = h(T_f - T_w) - \varepsilon_w \sigma T_w^{\,4} + \alpha_w \varepsilon_f \sigma T_f^{\,4} + \alpha_w (1-\alpha_f)\varepsilon_g \sigma T_g^{\,4}$$

It can be observed from Figure 27 that T_f reaches about 675K at the outlet, less than the wall temperature of 700K. A high fuel absorptivity α_f = 0.9 also translates into a reduction in the effect of the radiation from the gas core. Thus, with $T_f < T_w$ for the entire length, and a high fuel absorptivity limiting the radiation effect of the gas core, the overall heat flux to the wall can be negative, i.e. the heat transfer can be from the wall to the fuel.

G. DEVELOPMENT OF THE FUEL-GAS MIXING BOUNDARY LAYER

As the gas core is moving at a much faster velocity compared to the fuel layer, there is a shearing effect at the gas-fuel interface. Fuel sub-layers near the interface are constantly being sheared from the fuel layer, and mixed with the core gases. This forms the fuel mixing boundary layer, which grows along the length of the combustion chamber.

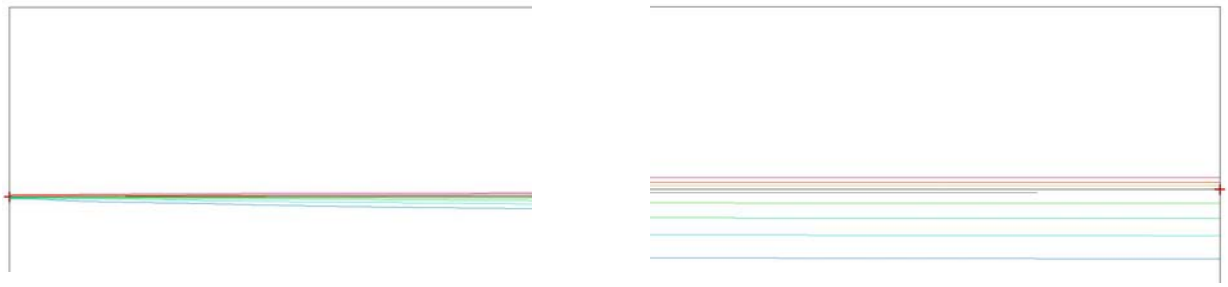

Figure 28. Development of the fuel-gas mixing boundary layer

Figure 28 shows how the fuel-gas mixing layer grows from the inlet to the outlet. The crosses on the inlet and outlet mark the initial horizontal line of the gas-fuel interface (y = 0.01805m). It grows or thickens as it moves from the inlet to the outlet. The observation that there is more mixing into the gas region indicates the shearing off of the fuel sub-layers near the interface into the gas core.

Several cases were run to see the effect on the growth of the fuel mixing boundary layer due to varying fuel absorptivities, wall temperatures, and fuel inlet velocities.

Varying parameter	Fuel absorptivity	Film cooling ratio (%)	Wall temperature (K)	
Fuel absorptivity	0.3	25.3	500	Case (1)
	0.9	25.3	500	Case (2)
Fuel inlet velocity	0.3	25.3	500	Case (1)
	0.3	14.4	500	Case (3)
Wall temperature	0.3	25.3	500	Case (1)
	0.3	25.3	900	Case (4)

Table 6. Parametric table for fuel mixing boundary layer growth

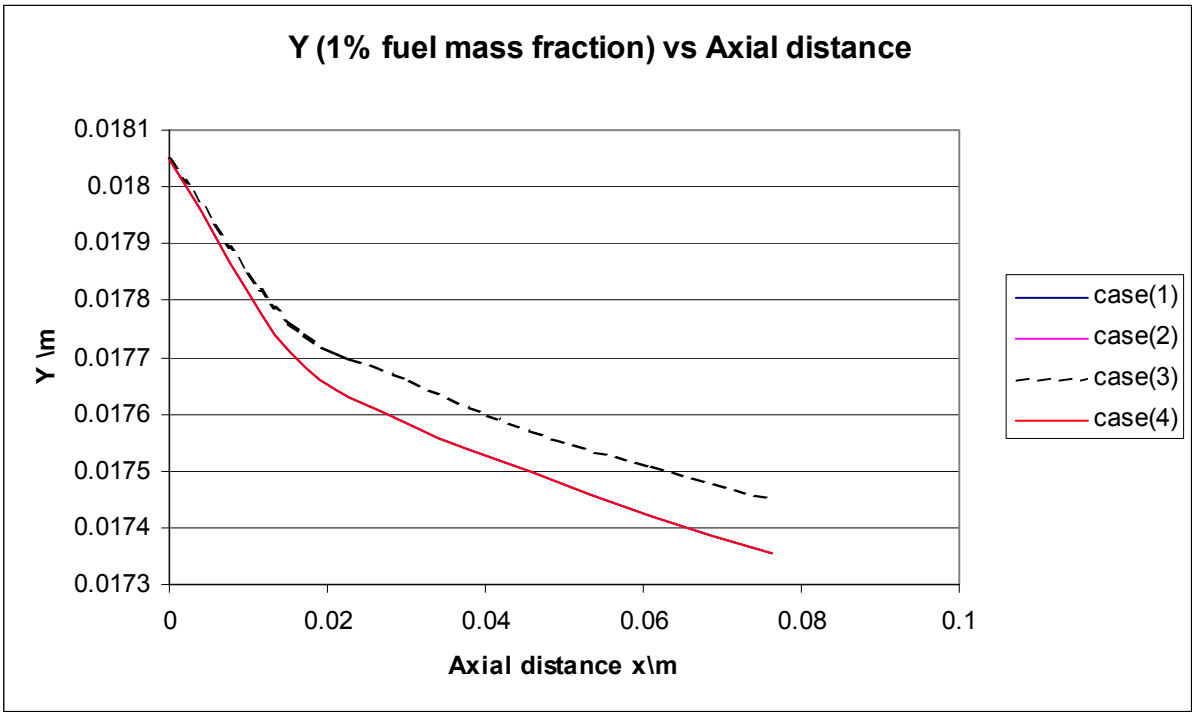

Figure 29. Fuel-gas mixing boundary layer growth into gas core

Figure 29 shows the growth of the fuel-gas mixing layer into the gas core based on the extent of the 1% fuel mass fraction boundary. Cases 1, 2 and 4 fall on the same line. This implies that fuel absorptivity and wall temperature have no significant effect on the growth of the fuel-gas mixing boundary layer. Case 3 falls on the dotted line, which has a lower growth rate of the fuel mixing boundary layer compared to the other cases. Though the fuel inlet velocity for case 3 is lower, the relative difference in velocity Δu at the interface is the same for all. However, the velocity ratio for case 3 is lower than the other cases. Hence, the rate of growth for the fuel-gas mixing layer into the gas core is less for lower velocity ratio of the fuel to gas flow speed. Hence, it can be concluded that the fuel-gas mixing layer growth is solely dependent on the flow properties of the fluids.

VI. CONCLUSIONS AND RECOMMENDATION

A numerical model and simulation has been developed for the combustion chamber of a liquid–fueled engine with an injected fuel film on the wall. In addition, the tendency of hydrocarbon fuels to produce soot precipitates at about 550K had been incorporated into the model and its effect evaluated numerically.

It was found that film cooling could effectively reduce the amount of heat flux to the chamber wall by at least 2 orders of magnitudes. This effect is critically dependent on the radiative absorptivity value of the fuel. An fuel film of high absorptivity is able to reduce the heat flux to the chamber wall by as much as 3 orders of magnitudes by effectively absorbing all the hot core gas radiation, and transmitting only minimally to the chamber wall. Therefore it may be worth exploring the option of using an optically thick fuel for film cooling, or alternatively to increase the absorptivity of the fuel, with additives or other means, so as to reduce the amount of heat flux to the chamber wall.

The fuel film absorbs heat primarily from the gas core through radiation and convection, and its bulk mean temperature increases from the inlet to the outlet. The rate of increase in the bulk mean temperature is greater for higher fuel absorptivity and lower fuel inlet velocity. The increase in the bulk mean temperature of the fuel layer between the inlet and the outlet ranges from 150K to 500K for the parameter range covered in this study.

Increasing the film-cooling ratio reduces the heat flux to the wall, hence resulting in an overall lower temperature of the entire wall. However, it is found that increasing the film-cooling ratio beyond 30% has little additional value in reducing the heat flux to the wall. Changes in heat flux to the wall are less sensitive to film cooling ratios, if the fuel absorptivity is higher. Thus, using a fuel

of higher absorptivity for film cooling will minimize the amount of fuel required for film cooling purposes.

It is found that increasing the relative difference (ΔT) between the wall temperature and fuel inlet temperature helps to reduce the amount of heat flux to the wall. Thus, the desired inner wall temperature should be set higher than the fuel inlet temperature, at values determined by safety and good engineering judgment.

In the study of the development of the fuel mixing boundary layer, it had been found that its development is determined primarily by the flow characteristics, especially the velocity ratio of the fuel film and the gas core.

More accurate and realistic estimates of the different effects of interest can be obtained by expanding the study to include the following:

- RP1 as a non-gray fuel with spectral optical properties.
- Modeling of the chamber wall (and material) with regenerative cooling on the exterior wall
- The interaction of the combustion mechanics with the flow and heat transfer characteristics
- The effect of the resulting non-uniform distribution of gaseous species in the chamber

APPENDIX A. TYPICAL OUTPUT OF TEP

1. Data inputs for the program and data extracted from the output file are in bold.

2. The TEP program is used to derive the various gas properties for CFD-ACE modelling and mole fractions for input into RADCAL.

3. In the TEP, the rocket application module is selected.

4. Under thermochemistry, the reactants, namely RP1 (JP-4)(fuel) and gaseous oxygen (oxidizer) are selected. The oxidizer-to-fuel (OF) ratio is set to 2.3.

5. For the thermospecies data, the master thermo file is selected.

6. Under the rocket operating conditions, the chamber pressure is set to 35 atmospheres and the chamber temperature is set to 3500K under the propellant energy specifications.

7. Thus the required inputs for TEP are namely,
    a. Reactants
    b. OF ratio
    c. Chamber pressure
    d. Chamber temperature

TYPICAL TEP OUTPUT

```
INPUT FILE:C:\PC_TEP_B\tep.dat
OUPUT FILE:C:\PC_TEP_B\tep.out
THERMODYNAMIC DATA FILE:C:\PC_TEP_B\species\thermo.dat
 TITLE
 DATA
  $DATA
  ODE=1,
  NZONES=1,
  NASUB=1,
  NASUP=1,
  $END
 REACTANTS
 C 1.     H 1.9423                                  100.    -5430.L  298.15F  .773
 O 2.                                               100.       0.0G  298.15O

 NAMELISTS
  $ODE
  RKT = .TRUE.
  PSIA=F,
  T(1)=3500,
  P(1)=35,
  OFSKED(1)=2.3,
  OF= T,
  $END

0TITLE
0DATA
      $DATA
      ODE=1,
      NZONES=1,
      NASUB=1,
      NASUP=1,
      $END
1


*********************************************************************************************
******************************

                          CALCULATE ODE AREA RATIO AND PRESSURE SCHEDULES FOR ZONE  1


*********************************************************************************************
******************************
 REACTANTS
 C   1.0000  H   1.9423      0.0000      0.0000      0.0000  100.000000      -
5430.00  L   298.150  F    0.77300
 O    2.0000       0.0000       0.0000       0.0000       0.0000   100.000000
0.00  G   298.150  O    0.00000
 NAMELISTS
      $ODE
      RKT = .TRUE.
      PSIA=F,
      T(1)=3500,
      P(1)=35,
      OFSKED(1)=2.3,
      OF= T,
      $END
0SPECIES BEING CONSIDERED IN THIS SYSTEM
     J 3/78  C              J12/67  CH             J12/72  CH2             J
3/61  CH2O             L 5/80  CH2O2
     J 6/69  CH3            BUR 84  CH2OH           L 6/80  CH3O            L
5/84  CH4              L 4/80  CH3OH
     J 9/65  CO             J 9/65  CO2            J12/69  C2              J
3/67  C2H              J 3/61  C2H2
```

```
            B 76    C2H3             L 4/80  C2H4             L 5/80  C2H4O2           L
5/80  C2H4O4           L 8/78  C2H5
            L 5/84  C2H6             BUR 84  C2H5OH           BUR 84  CH3OCH3          J
9/66  C2O              J12/69  C3
            B 76     C3H6                  L11/80   C3H6O                BUR 84   N-C3H7
BUR 84  I-C3H7           L 4/80  C3H8
            L 1/84  1-C3H7OH         J 6/68  C3O2             J12/69  C4               L
5/80  C4H8O4           L 4/80  N-C4H10
            L 5/80  I-C4H10          J12/69  C5               L 1/84  C6H5             L
1/84  C6H6             EID  9  C7H14
            L  6/88   JET-A(G)              DR     9   C12H26                  J  3/77   H
J12/70  HCO              J 9/78  HO2
            J 3/77  H2               J 3/79  H2O              L 6/80  H2O2             J
6/66  H3O              J 3/77  O
            J 6/77  OH               J 3/77  O2               J 6/61  O3               J
3/78  C(GR)            Est.99  JP10(L)
            L 6/88  JET-A(L)         P1   9  C12H26(L)        L 3/81  H2O(S)           J
3/79  H2O(L)
       0OF =   2.300000
                                EFFECTIVE  FUEL                        EFFECTIVE  OXIDANT
MIXTURE
        ENTHALPY                                HPP(2)                              HPP(1)
HSUB0
        (KG-MOL)(DEG K)/KG       -0.19573987E+03             0.00000000E+00            -
0.59315113E+02
       0KG-ATOMS/KG                           B0P(I,2)                            B0P(I,1)
B0(I)
              C                           0.71587443E-01                0.00000000E+00
0.21693164E-01
              H                           0.13904428E+00                0.00000000E+00
0.42134631E-01
              O                           0.00000000E+00                0.62502339E-01
0.43562237E-01

        ENTHALPY IN BTU/LBM :
            FROM REACTANTS :       -212.0290
            FROM DELH( )   :          0.0000
            FROM DELH1( )  :          0.0000
            TOTAL          :       -212.0290
       1                                                    ZONE =  1
                              THEORETICAL   ROCKET   PERFORMANCE   ASSUMING   EQUILIBRIUM
COMPOSITION DURING EXPANSION

                                                      FROM   AN   ASSIGNED   PRESSURE   AND
TEMPERATURE
       0PC =   514.4 PSIA
                                                                                      WT
FRACTION  ENTHALPY  STATE   TEMP    DENSITY
                 CHEMICAL FORMULA                                                    (SEE
NOTE) JOULES/MOL          DEG K   KG/M3
        FUEL                       C           1.00000                H           1.94230
1.00000   -22719.119    L    298.15 773.0000
       OXIDANT                     O                                              2.00000
1.00000        0.000    G    298.15   0.0000
       0O/F=2.3000E+00   PERCENT  FUEL=3.0303E+01   EQUIVALENCE  RATIO=1.4796E+00   STOIC
MIXTURE RATIO=3.4030E+00  DENSITY=0.0000E+00
       0               CHAMBER   THROAT
        PC/P             1.0000   1.7370
        P, N/M2        3.5464 6 2.0416 6
        T, DEG K           3500     3308
        H, J/KG       -8.2452 5-1.5241 6
        S, J/(KG)(K)   1.1776 4 1.1776 4
        G, CAL/GRAM    -10048.1  -9673.6
        U, CAL/GRAM      -510.5   -656.7
        DEN, (KG/M3)    2.70     1.67

        M, MOL WT        22.177   22.460
        (DLV/DLP)T     -1.02948 -1.02279
        (DLV/DLT)P       1.5263   1.4308
```

CP, J/(KG)(K	**5.6278 3**	5.1079 3
CP GAS(SF)	0.4936	0.4911
GAMMA GAS(SF)	1.2216	1.2196
GAMMA (S)	1.1437	1.1435
SON VEL,M/SEC	**1225.0**	1183.2
MU, POISE	**9.36E-04**	9.01E-04
K,ERG/S-CM-K	3.38E+04	3.22E+04
PRANDTL NO	**0.57222**	0.57629
MACH NUMBER	0.0000	1.0000

AE/AT	1.0000
CSTAR, M/SEC	1797
CF VAC	1.234
CF	0.658
IVAC,N-S/KG	2218.01
I, N-S/KG	1183.24
MOL WT(MIX)	22.177 22.460

MOLE FRACTIONS

CH2O	**0.000001**	**0.000000**
CH2O2	**0.000002**	**0.000001**
CO	**0.365959**	**0.363557**
CO2	**0.115107**	**0.123662**
H	**0.034555**	**0.028708**
HCO	**0.000022**	**0.000012**
HO2	**0.000043**	**0.000023**
H2	**0.121314**	**0.121240**
H2O	**0.307796**	**0.321470**
H2O2	**0.000005**	**0.000002**
O	**0.006833**	**0.004468**
OH	**0.041569**	**0.032179**
O2	**0.006795**	**0.004676**

MASS FRACTIONS

CH2O	0.000001	0.000001
CH2O2	0.000003	0.000002
CO	0.462222	0.453399
CO2	0.228428	0.242312
H	0.001571	0.001288
HCO	0.000029	0.000016
HO2	0.000065	0.000033
H2	0.011028	0.010882
H2O	0.250035	0.257852
H2O2	0.000007	0.000004
O	0.004930	0.003183
OH	0.031879	0.024367
O2	0.009804	0.006662

0ADDITIONAL PRODUCTS WHICH WERE CONSIDERED BUT WHOSE MOLE FRACTIONS WERE LESS THAN .0000005 FOR ALL ASSIGNED CONDITIONS

C CH CH2 CH3 CH2OH CH3O CH4
CH3OH C2 C2H
C2H2 C2H3 C2H4 C2H4O2 C2H4O4 C2H5
C2H6 C2H5OH CH3OCH3 C2O
C3 C3H6 C3H6O N-C3H7 I-C3H7 C3H8 1-
C3H7OH C3O2 C4 C4H8O4
N-C4H10 I-C4H10 C5 C6H5 C6H6 C7H14
JET-A(G) C12H26 H3O O3
C(GR) JP10(L) JET-A(L) C12H26(L) H2O(S) H2O(L)

NOTE
WEIGHT FRACTION OF FUEL IN TOTAL FUELS AND OF OXIDANT IN TOTAL OXIDANTS
(SF) STANDS FOR (SHIFTING FROZEN)

1
0 FROZEN TRANSPORT PROPERTIES CALCULATED FROM EQUILIBRIUM CONCENTRATIONS

```
            STATION                   MU                  K                   PR
                                  (LBF-SEC/FT**2)     (LBF/SEC-DEG R)
            CHAMBER             1.95878397E-06      4.22667153E-02      5.72215974E-01
            THROAT              1.88504566E-06      4.01893072E-02      5.76288342E-01
            EXIT                1.17292245E-06      2.25525107E-02      5.77992916E-01
       0      VISCOSITY  EXPONENT  (OMEGA)  FOR  THE  FORM  MU=MUREF*(T/TREF)**OMEGA  IS
0.68445
          MUREF FOR INPUT TO BLM=   6.30434442E-05 LBM/(FT-SEC)
       0          SPECIES CONSIDERED IN TRANSPORT PROPERTIES CALCULATIONS
                  C                   CH                  CH4                 CH3OH
                  CO                  CO2                 C2                  C2H2
                  C2H4                C2H6                C2H5OH              CH3OCH3
                  C3H8                N-C4H10             C6H6                H
                  H2                  H2O                 H2O2                O
                  OH                  O2
       1                                                        ZONE =  1
                                 THEORETICAL   ROCKET   PERFORMANCE   ASSUMING   FROZEN
COMPOSITION DURING EXPANSION

                                                      FROM   AN   ASSIGNED   PRESSURE   AND
TEMPERATURE
       0PC =  3546375.0 N/M2
                                                                                      WT
FRACTION  ENTHALPY  STATE   TEMP    DENSITY
                CHEMICAL FORMULA                                                       (SEE
NOTE) JOULES/MOL          DEG K   KG/M3
        FUEL                      C           1.00000               H           1.94230
1.00000   -22719.119    L    298.15 773.0000
        OXIDANT                   O                                             2.00000
1.00000       0.000    G    298.15   0.0000
       0O/F=2.3000E+00   PERCENT  FUEL=3.0303E+01   EQUIVALENCE  RATIO=1.4796E+00   STOIC
MIXTURE RATIO=3.4030E+00  DENSITY=0.0000E+00
       0                CHAMBER   THROAT
        PC/P             1.0000   1.7867
        P, N/M2        3.5464 6 1.9849 6
        T, DEG K           3500     3148
        H, J/KG       -8.2452 5-1.5468 6
        S, J/(KG)(K)   1.1776 4 1.1776 4
        G, CAL/GRAM    -10048.1  -9231.3
        U, CAL/GRAM      -510.5   -651.6
        DEN, (KG/M3)   2.70     1.68

        M, MOL WT        22.177   22.177
        CP, J/(KG)(K   2.0651 3 2.0435 3
        GAMMA (S)        1.2216   1.2245
        SON VEL,M/SEC    1266.1   1202.2
        MACH NUMBER      0.0000   1.0000

        AE/AT                    1.0000
        CSTAR, M/SEC               1754
        CF  VAC                  1.245
        CF                       0.685
        IVAC,N-S/KG             2184.06
        I, N-S/KG               1202.24

        MOLE FRACTIONS

        CH2O          0.000001       CH2O2         0.000002       CO            0.365959
CO2          0.115107
        H             0.034555       HCO           0.000022       HO2           0.000043
H2           0.121314
        H2O           0.307796       H2O2          0.000005       O             0.006833
OH           0.041569
        O2           0.006795

        MASS FRACTIONS
```

```
         CH2O          0.000001        CH2O2         0.000003        CO            0.462222
CO2           0.228428
         H             0.001571        HCO           0.000029        HO2           0.000065
H2            0.011028
         H2O           0.250035        H2O2          0.000007        O             0.004930
OH            0.031879
         O2           0.009804
        0ADDITIONAL PRODUCTS WHICH WERE CONSIDERED BUT WHOSE MOLE FRACTIONS WERE LESS THAN
.0000005 FOR ALL ASSIGNED CONDITIONS
         C             CH           CH2          CH3          CH2OH        CH3O          CH4
CH3OH         C2           C2H
         C2H2            C2H3            C2H4            C2H4O2         C2H4O4         C2H5
C2H6          C2H5OH        CH3OCH3       C2O
         C3            C3H6          C3H6O         N-C3H7        I-C3H7        C3H8          1-
C3H7OH     C3O2          C4            C4H8O4
         N-C4H10        I-C4H10        C5              C6H5            C6H6            C7H14
JET-A(G)      C12H26        H3O           O3
         C(GR)         JP10(L)       JET-A(L)      C12H26(L)     H2O(S)        H2O(L)

         NOTE
                WEIGHT FRACTION OF FUEL IN TOTAL FUELS AND OF OXIDANT IN TOTAL OXIDANTS
        1


********************************************************************************************
*******************************

                          CALCULATE ODE AREA RATIO AND PRESSURE SCHEDULES FOR ZONE  1

********************************************************************************************
*******************************

         *** EOF ENCOUNTERED IN READING ODE REACTANTS DATA ***

                  *********CPU(SEC) =             0.2 **********
```

APPENDIX B. DETERMINATION OF THE SPECTRAL BANDS

1. The purpose of RADCAL is to obtain the spectral bands of the radiation of the combustion gases. The outputs required from RADCAL are the wavelengths (microns) and the transmissivity (tau). Since (1-tau) equals absorptivity, the required plot is (1-tau) versus wavelength. From the plot, the number of bands and their bandwidths can be determined.

2. The required inputs are namely, the average mean beam length, partial pressures of the constituent gases and wall temperature.

3. The average mean beam length is calculated with reference to M.F. Modest, Table 17.1 pg 593 [2]. The height-to-diameter ratio is calculated, which equals to 2. Since the surface in consideration is the wall, i.e. concave surface, the ratio L_m/L equals 0.76.

$$L_m = 0.76L = 0.76(0.0762) = 0.0579m$$

4. The partial pressures (kPa) are calculated by multiplying the mole fractions of the gases (from TEP) by the total chamber pressure. A sample of the Excel spreadsheet is shown below.

TOTAL PRESSURE			MOLE	PARTIAL	
atm	kPa		FRACTION	PRESSURE	
35	3546.375	C02	0.115	407.833	
35	3546.375	H2O	0.308	1092.280	
35	3546.375	CH4	0	0	
35	3546.375	CO	0.367	1301.520	
35	3546.375	O2	0.007	24.820	
35	3546.375	N2	0.203	719.910	remainder

Table 7. Calculation of partial pressures of constituent gases

5. The wall temperature is set to 500K.

6. The RADCAL output file can be imported into an Excel spreadsheet. The wavelength (micron) is plotted against (1-tau) in the Excel spreadsheet as shown:

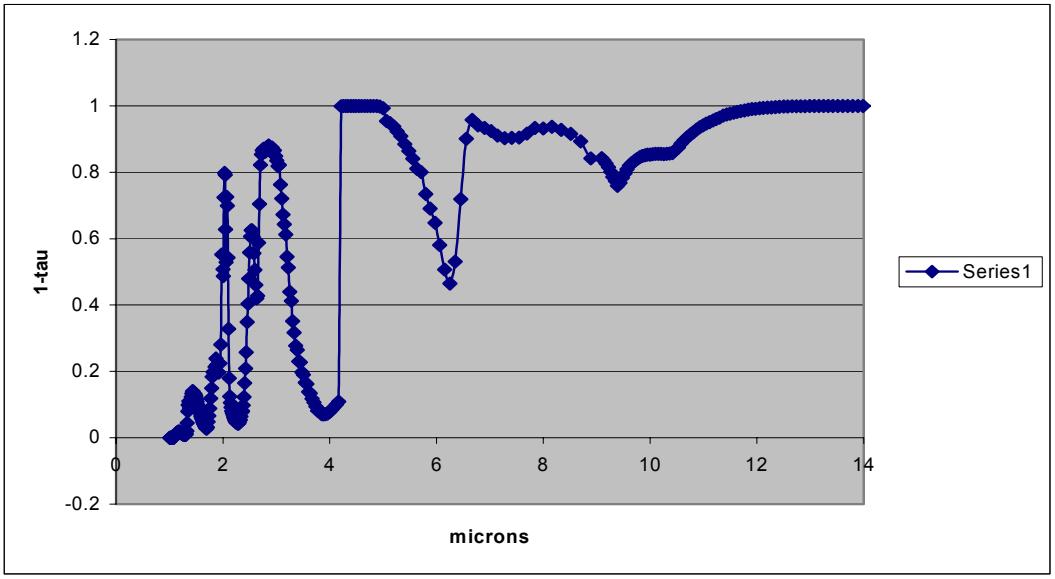

Figure 30. RADCAL plot

7. From the plot, the spectral bands can be determined as follows:

	wavelength (in micrometers)	
band	**limit1**	**limit2**
1	0	1.3
2	1.3	1.7
3	1.7	1.9
4	1.9	2.3
5	2.3	2.6
6	2.6	4
7	4	6.25
8	6.25	9.4
9	9.4	inf

Table 8. Computation of the spectral bands

8. A typical RADCAL output file is shown below. The inputs are in **bold.**

TYPICAL RADCAL OUTPUT FILE

Radial Profiles

Partial Pressures, kPa

J	dist,m	temp,K	CO2	H2O	CH4	CO	O2	N2	FV
1	**.0579**	**3500.**	**407.833**	**1092.280**	**.000**	**1301.520**	**24.820**	**719.910**	**.0000E+00**
wall		**500.**							

Total directional radiated energy flux = .334840E+06 Watts/m-2/strad

Spectral Intensity Distribution, Watts/m-2/micron/strad

micron	intensity	tau	micron	intensity	tau
1.005	.4268E-04	1.0000	6.061	.8768E+04	.4193
1.010	.4806E-04	1.0000	6.154	.7266E+04	.4927
1.015	.5411E-04	1.0000	6.250	.6303E+04	.5354
1.020	.6091E-04	1.0000	6.349	.6787E+04	.4691
1.026	.6856E-04	1.0000	6.452	.8636E+04	.2806
1.031	.7716E-04	1.0000	6.557	.1017E+05	.0986
1.036	.8683E-04	1.0000	6.667	.1016E+05	.0423
1.042	.9769E-04	1.0000	6.780	.9399E+04	.0582
1.047	.1099E-03	1.0000	6.897	.8752E+04	.0664
1.053	.1236E-03	1.0000	7.018	.8134E+04	.0753
1.058	.1390E-03	1.0000	7.143	.7509E+04	.0891
1.064	.1563E-03	1.0000	7.273	.6968E+04	.0968
1.070	.1758E-03	1.0000	7.407	.6516E+04	.0962
1.075	.1976E-03	1.0000	7.547	.6086E+04	.0955
1.081	.5529E+04	.9970	7.692	.5746E+04	.0834
1.087	.6137E+04	.9966	7.843	.5445E+04	.0662
1.093	.7516E+04	.9959	8.000	.5051E+04	.0677
1.099	.9417E+04	.9948	8.163	.4708E+04	.0632
1.105	.1197E+05	.9933	8.333	.4317E+04	.0725
1.111	.1561E+05	.9912	8.511	.3942E+04	.0840
1.117	.1876E+05	.9894	8.696	.3550E+04	.1068
1.124	.2092E+05	.9881	8.889	.3088E+04	.1578
1.130	.2279E+05	.9869	9.091	.2841E+04	.1570
1.136	.2497E+05	.9856	9.132	.2770E+04	.1643
1.143	.2694E+05	.9843	9.174	.2694E+04	.1734
1.149	.2821E+05	.9835	9.217	.2613E+04	.1846
1.156	.2979E+05	.9824	9.259	.2527E+04	.1981
1.163	.3028E+05	.9820	9.302	.2435E+04	.2142
1.170	.3028E+05	.9819	9.346	.2357E+04	.2264
1.176	.3051E+05	.9816	9.390	.2276E+04	.2403
1.183	.3058E+05	.9814	9.434	.2259E+04	.2321
1.190	.3032E+05	.9814	9.479	.2262E+04	.2167
1.198	.2851E+05	.9823	9.524	.2259E+04	.2035
1.205	.2650E+05	.9834	9.569	.2253E+04	.1906
1.212	.2436E+05	.9846	9.615	.2241E+04	.1801
1.220	.2262E+05	.9856	9.662	.2222E+04	.1716
1.227	.2069E+05	.9867	9.709	.2199E+04	.1651

1.235	.1923E+05	.9875	9.756	.2171E+04	.1603
1.242	.1787E+05	.9883	9.804	.2145E+04	.1549
1.250	.1623E+05	.9893	9.852	.2115E+04	.1510
1.258	.1535E+05	.9897	9.901	.2081E+04	.1485
1.266	.1448E+05	.9902	9.950	.2046E+04	.1472
1.274	.1383E+05	.9906	10.000	.2008E+04	.1470
1.282	.1355E+05	.9907	10.050	.1975E+04	.1453
1.290	.1271E+05	.9912	10.101	.1939E+04	.1444
1.299	.1277E+05	.9910	10.152	.1903E+04	.1442
1.307	.1311E+05	.9907	10.204	.1866E+04	.1446
1.316	.1726E+05	.9876	10.256	.1829E+04	.1454
1.325	.2879E+05	.9790	10.309	.1795E+04	.1446
1.333	.6119E+05	.9549	10.363	.1762E+04	.1438
1.342	.1074E+06	.9199	10.417	.1732E+04	.1418
1.351	.1314E+06	.9008	10.471	.1714E+04	.1334
1.361	.1435E+06	.8903	10.526	.1695E+04	.1253
1.370	.1276E+06	.9013	10.582	.1682E+04	.1139
1.379	.1141E+06	.9106	10.638	.1667E+04	.1036
1.389	.1149E+06	.9088	10.695	.1650E+04	.0944
1.399	.1390E+06	.8882	10.753	.1631E+04	.0862
1.408	.1508E+06	.8770	10.811	.1610E+04	.0789
1.418	.1616E+06	.8664	10.870	.1590E+04	.0714
1.429	.1674E+06	.8597	10.929	.1568E+04	.0648
1.439	.1651E+06	.8597	10.989	.1545E+04	.0589
1.449	.1579E+06	.8639	11.050	.1521E+04	.0537
1.460	.1513E+06	.8677	11.111	.1496E+04	.0491
1.471	.1505E+06	.8664	11.173	.1472E+04	.0441
1.481	.1455E+06	.8689	11.236	.1448E+04	.0396
1.493	.1373E+06	.8744	11.299	.1423E+04	.0356
1.504	.1255E+06	.8834	11.364	.1401E+04	.0297
1.515	.1157E+06	.8908	11.429	.1375E+04	.0262
1.527	.1053E+06	.8990	11.494	.1350E+04	.0232
1.538	.9770E+05	.9048	11.561	.1324E+04	.0207
1.550	.9029E+05	.9105	11.628	.1298E+04	.0181
1.563	.8038E+05	.9190	11.696	.1273E+04	.0156
1.575	.7199E+05	.9262	11.765	.1247E+04	.0136
1.587	.6292E+05	.9344	11.834	.1221E+04	.0116
1.600	.5492E+05	.9417	11.905	.1196E+04	.0100
1.613	.4840E+05	.9477	11.976	.1171E+04	.0085
1.626	.4306E+05	.9526	12.048	.1146E+04	.0072
1.639	.3786E+05	.9576	12.121	.1120E+04	.0063
1.653	.3256E+05	.9628	12.195	.1096E+04	.0052
1.667	.2850E+05	.9668	12.270	.1071E+04	.0044
1.681	.2449E+05	.9709	12.346	.1047E+04	.0036
1.695	.2315E+05	.9720	12.422	.1023E+04	.0029
1.709	.2614E+05	.9677	12.500	.1000E+04	.0022
1.724	.3855E+05	.9514	12.579	.9768E+03	.0017
1.739	.5171E+05	.9335	12.658	.9538E+03	.0014
1.754	.6742E+05	.9114	12.739	.9311E+03	.0011
1.770	.8815E+05	.8817	12.821	.9088E+03	.0009
1.786	.1093E+06	.8501	12.903	.8869E+03	.0007
1.802	.1312E+06	.8160	12.987	.8653E+03	.0004
1.818	.1385E+06	.8015	13.072	.8440E+03	.0003
1.835	.1332E+06	.8046	13.158	.8232E+03	.0002
1.852	.1428E+06	.7857	13.245	.8026E+03	.0002
1.869	.1554E+06	.7613	13.333	.7825E+03	.0001
1.887	.1401E+06	.7797	13.423	.7626E+03	.0001
1.905	.1238E+06	.8005	13.514	.7432E+03	.0001
1.923	.1193E+06	.8029	13.605	.7241E+03	.0000
1.942	.1326E+06	.7755	13.699	.7054E+03	.0000
1.961	.1620E+06	.7186	13.793	.6870E+03	.0000
1.980	.3097E+06	.4480	13.889	.6690E+03	.0000

2.000	.2775E+06	.4922	13.986	.6513E+03	.0000
2.010	.2628E+06	.5126	14.085	.6339E+03	.0000
2.020	.3854E+06	.2757	14.184	.6169E+03	.0000
2.030	.4188E+06	.2023	14.286	.6003E+03	.0000
2.041	.4101E+06	.2080	14.388	.5839E+03	.0000
2.051	.3206E+06	.3723	14.493	.5679E+03	.0000
2.062	.2665E+06	.4710	14.599	.5522E+03	.0000
2.073	.3608E+06	.2738	14.706	.5369E+03	.0000
2.083	.3424E+06	.3010	14.815	.5218E+03	.0000
2.094	.2622E+06	.4571	14.925	.5071E+03	.0000
2.105	.1563E+06	.6718	15.038	.4926E+03	.0000
2.116	.8424E+05	.8205	15.152	.4785E+03	.0000
2.128	.5758E+05	.8755	15.267	.4646E+03	.0000
2.139	.4816E+05	.8944	15.385	.4511E+03	.0000
2.151	.4124E+05	.9082	15.504	.4379E+03	.0000
2.162	.3586E+05	.9190	15.625	.4249E+03	.0000
2.174	.3257E+05	.9253	15.748	.4122E+03	.0000
2.186	.2994E+05	.9303	15.873	.3998E+03	.0000
2.198	.2660E+05	.9371	16.000	.3877E+03	.0000
2.210	.2409E+05	.9422	16.129	.3758E+03	.0000
2.222	.2183E+05	.9468	16.260	.3642E+03	.0000
2.235	.2000E+05	.9505	16.393	.3529E+03	.0000
2.247	.1841E+05	.9537	16.529	.3418E+03	.0000
2.260	.1746E+05	.9554	16.667	.3310E+03	.0000
2.273	.1681E+05	.9563	16.807	.3205E+03	.0000
2.286	.1586E+05	.9581	16.949	.3102E+03	.0000
2.299	.1639E+05	.9560	17.094	.3001E+03	.0000
2.312	.1815E+05	.9505	17.241	.2903E+03	.0000
2.326	.1969E+05	.9454	17.391	.2807E+03	.0000
2.339	.2278E+05	.9357	17.544	.2714E+03	.0000
2.353	.2683E+05	.9230	17.699	.2623E+03	.0000
2.367	.2761E+05	.9194	17.857	.2534E+03	.0000
2.381	.3313E+05	.9017	18.018	.2447E+03	.0000
2.395	.4060E+05	.8774	18.182	.2362E+03	.0000
2.410	.5375E+05	.8348	18.349	.2280E+03	.0000
2.424	.6675E+05	.7912	18.519	.2200E+03	.0000
2.439	.8082E+05	.7426	18.692	.2122E+03	.0000
2.454	.1075E+06	.6514	18.868	.2046E+03	.0000
2.469	.1222E+06	.5965	19.048	.1972E+03	.0000
2.484	.1425E+06	.5207	19.231	.1900E+03	.0000
2.500	.1630E+06	.4416	19.417	.1830E+03	.0000
2.516	.1739E+06	.3933	19.608	.1762E+03	.0000
2.532	.1758E+06	.3748	19.802	.1695E+03	.0000
2.548	.1725E+06	.3750	20.000	.1631E+03	.0000
2.564	.1641E+06	.3937	20.202	.1568E+03	.0000
2.581	.1476E+06	.4443	20.408	.1507E+03	.0000
2.597	.1317E+06	.4943	20.619	.1448E+03	.0000
2.614	.1176E+06	.5394	20.833	.1391E+03	.0000
2.632	.1051E+06	.5801	21.053	.1335E+03	.0000
2.649	.1051E+06	.5718	21.277	.1281E+03	.0000
2.667	.1414E+06	.4121	21.505	.1229E+03	.0000
2.685	.1660E+06	.2956	21.739	.1178E+03	.0000
2.703	.1899E+06	.1776	21.978	.1129E+03	.0000
2.721	.1931E+06	.1460	22.222	.1081E+03	.0000
2.740	.1918E+06	.1338	22.472	.1035E+03	.0000
2.759	.1889E+06	.1287	22.727	.9906E+02	.0000
2.778	.1843E+06	.1319	22.989	.9473E+02	.0000
2.797	.1792E+06	.1374	23.256	.9054E+02	.0000
2.817	.1780E+06	.1245	23.529	.8650E+02	.0000
2.837	.1742E+06	.1239	23.810	.8258E+02	.0000
2.857	.1712E+06	.1198	24.096	.7881E+02	.0000
2.878	.1660E+06	.1272	24.390	.7515E+02	.0000

2.899	.1618E+06	.1298	24.691	.7163E+02	.0000
2.920	.1589E+06	.1258	25.000	.6823E+02	.0000
2.941	.1532E+06	.1376	25.316	.6495E+02	.0000
2.963	.1503E+06	.1339	25.641	.6179E+02	.0000
2.985	.1438E+06	.1516	25.974	.5874E+02	.0000
3.008	.1382E+06	.1654	26.316	.5581E+02	.0000
3.030	.1323E+06	.1814	26.667	.5298E+02	.0000
3.053	.1297E+06	.1782	27.027	.5027E+02	.0000
3.077	.1174E+06	.2375	27.397	.4765E+02	.0000
3.101	.1083E+06	.2795	27.778	.4514E+02	.0000
3.125	.9864E+05	.3270	28.169	.4273E+02	.0001
3.150	.9199E+05	.3565	28.571	.4042E+02	.0001
3.175	.8539E+05	.3873	28.986	.3820E+02	.0001
3.200	.7414E+05	.4542	29.412	.3607E+02	.0001
3.226	.6793E+05	.4868	29.851	.3403E+02	.0002
3.252	.5676E+05	.5599	30.303	.3207E+02	.0002
3.279	.5176E+05	.5879	30.769	.3020E+02	.0003
3.306	.4302E+05	.6483	31.250	.2841E+02	.0004
3.333	.3776E+05	.6829	31.746	.2670E+02	.0005
3.361	.3215E+05	.7226	32.258	.2507E+02	.0006
3.390	.2980E+05	.7357	32.787	.2351E+02	.0008
3.419	.2525E+05	.7698	33.333	.2203E+02	.0010
3.448	.2431E+05	.7721	33.898	.2061E+02	.0013
3.478	.2049E+05	.8024	34.483	.1926E+02	.0017
3.509	.1913E+05	.8103	35.088	.1798E+02	.0021
3.540	.1631E+05	.8335	35.714	.1676E+02	.0027
3.571	.1545E+05	.8376	36.364	.1560E+02	.0035
3.604	.1283E+05	.8612	37.037	.1450E+02	.0045
3.636	.1204E+05	.8659	37.736	.1345E+02	.0058
3.670	.1028E+05	.8821	38.462	.1246E+02	.0074
3.704	.9025E+04	.8933	39.216	.1152E+02	.0096
3.738	.7787E+04	.9052	40.000	.1062E+02	.0125
3.774	.6532E+04	.9181	40.816	.9781E+01	.0157
3.810	.6468E+04	.9163	41.667	.8982E+01	.0199
3.846	.5368E+04	.9285	42.553	.8226E+01	.0251
3.883	.5135E+04	.9294	43.478	.7510E+01	.0317
3.922	.5035E+04	.9285	44.444	.6832E+01	.0402
3.960	.4996E+04	.9267	45.455	.6199E+01	.0492
4.000	.5126E+04	.9221	46.512	.5602E+01	.0602
4.040	.5435E+04	.9145	47.619	.5039E+01	.0738
4.082	.5711E+04	.9070	48.780	.4508E+01	.0905
4.124	.5981E+04	.8990	50.000	.4008E+01	.1111
4.167	.6244E+04	.8907	51.282	.3557E+01	.1304
4.211	.5433E+05	.0010	52.632	.3136E+01	.1531
4.255	.5243E+05	.0002	54.054	.2744E+01	.1799
4.301	.5054E+05	.0000	55.556	.2380E+01	.2115
4.348	.4869E+05	.0000	57.143	.2043E+01	.2488
4.396	.4689E+05	.0000	58.824	.1759E+01	.2791
4.444	.4513E+05	.0000	60.606	.1500E+01	.3132
4.494	.4341E+05	.0000	62.500	.1266E+01	.3516
4.545	.4174E+05	.0000	64.516	.1055E+01	.3947
4.598	.4011E+05	.0000	66.667	.8658E+00	.4433
4.651	.3852E+05	.0000	68.966	.7166E+00	.4804
4.706	.3698E+05	.0000	71.429	.5855E+00	.5206
4.762	.3548E+05	.0000	74.074	.4712E+00	.5642
4.819	.3401E+05	.0001	76.923	.3724E+00	.6116
4.878	.3258E+05	.0005	80.000	.2879E+00	.6631
4.938	.3115E+05	.0021	83.333	.2289E+00	.6946
5.000	.2968E+05	.0066	86.957	.1792E+00	.7277
5.063	.2727E+05	.0459	90.909	.1378E+00	.7624
5.128	.2590E+05	.0520	95.238	.1037E+00	.7988
5.195	.2449E+05	.0620	100.000	.7615E-01	.8370

5.263	.2301E+05	.0767	105.263	.5840E-01	.8560
5.333	.2161E+05	.0908	111.111	.4405E-01	.8755
5.405	.2006E+05	.1149	117.647	.3261E-01	.8954
5.479	.1866E+05	.1357	125.000	.2363E-01	.9158
5.556	.1729E+05	.1591	133.333	.1670E-01	.9367
5.634	.1585E+05	.1895	142.857	.1217E-01	.9462
5.714	.1488E+05	.1995	153.846	.8672E-02	.9559
5.797	.1298E+05	.2655	166.667	.6019E-02	.9656
5.882	.1159E+05	.3093	181.818	.4052E-02	.9755
5.970	.1031E+05	.3521	200.000	.2631E-02	.9855

The effective absorption coef. is .227224E+01/m
The Planck-mean absorption coef. is .740767E+01/m
The wall-incident mean is .973803E+02/m

THIS PAGE INTENTIONALLY LEFT BLANK

APPENDIX C. CALCULATION OF THE ABSORPTION COEFFICIENTS

The box model developed by Penner[3] is adopted due to its great simplicity, as in many other researches.

In using the box model, $\Delta\eta_e$ is obtained using RADCAL and therefore $\bar{\kappa}$ is assumed to be related to the band intensity α by

$$\bar{\kappa} = \frac{\alpha}{\Delta\eta_e}$$

The band intensity α is obtained using the Exponential Wide Band model. Modest presents a very useful table for Wide band model correlation parameters for various gases (Table 9.3, p352).

For a given spectral band, the dominant gas contributing to radiation is determined using Table 9.3, by comparing their reference band intensities α_0. As there is temperature dependence in the strength parameter for the various gases, the actual band intensity α is calculated by multiplying the normalized band strength parameter with α_0. The normalized band strength parameter can be obtained from graphs in Modest (p 356-357).

Since the band intensity α_0 has the units $[cm^{-1}/(g/m^2)]$, it will result in mass absorption coefficient. Hence there is a need to multiply by the density of the gas to attain the actual absorption coefficient [m^{-1}] to input for CFD-ACE.

A sample calculation is shown below:

Spectral band : 4 μm – 6.25 μm, thus dominant gas is CO2 at 4.3 μm.

For CO2 at 4.3 μm, α_0 = 110.0 $[cm^{-1}/(g/m^2)]$

At 3500K, $\frac{T}{T_0} = \frac{3500}{100} = 35$

Referring to Figure 9-13 in Modest, $\frac{\alpha}{\alpha_0} = 1.0$ for 4.3 μm

To calculate the density of CO2, assuming ideal gas,

$$\rho_{CO2} = \frac{x.P_{CO2}}{R.T}$$

@35 atm, with mole fraction x = 0.115 (from TEP),

$$R = \frac{8.314\_[J/mol.K]}{44\_[g/mol]} = 0.189\_[J/g.K]$$

Therefore, $$\rho_{CO2} = \frac{x.P_{CO2}}{R.T} = \frac{0.115x35x1.01325e5\_[J/m^3]}{0.189\_[J/g.K]x3500\_[K]} = 616.67\_[g/m^3]$$

Using the box model,

$$\bar{\kappa} = \frac{\alpha}{\Delta\eta_e} = \frac{110\_[cm^{-1}/(g/m^2)]x616.67\_[g/m^3]}{\left(\frac{1}{4} - \frac{1}{6.25}\right)10^4\_[cm^{-1}]} = 75.37m^{-1}$$

APPENDIX D. TYPICAL CFDACE OUTPUT FILE

```
************************************************************
**                                                        **
**   CCCCC  FFFFF  DDDD        AAA   CCCCC  EEEEE  U   U   **
**   C      F      D   D      A   A  C      E      U   U   **
**   C      FFFF   D   D  ==  AAAAA  C      EEEE   U   U   **
**   C      F      D   D      A   A  C      E      U   U   **
**   CCCCC  F      DDDD       A   A  CCCCC  EEEEE   UUU    **
**                                                        **
**       Version          : 2002. 0.27                    **
**       Build Date       : 07/28/2002 22:34:49           **
**       Build OS         : Windows_NT                    **
**       Build OS Release : 1.3.12(0.54/3/2)              **
**       Build OS Version : 2002-07-06 02:16              **
**       Build Machine    : BELL2                         **
**                                                        **
**      Copyright (c) 2000, CFD Research Corporation,     **
**                   All Rights Reserved                  **
************************************************************


================================================================
   CFD-ACEU Run Platform Information :
================================================================
   Run Date           : 11/05/2003 17:10:02
   Run OS             : Windows
   Run OS Release     :
   Run OS Version     :
   Run Machine        : IT002092
================================================================


 ====================================
 Summary of Input Information
 ====================================

 Title              :
 Modules            : FLOW HEAT TURBULENCE RADIATION
 DTF File Name      : fuel500K_vel30_adiabatic_0.3_i

 Model Name         : fuel500K_vel30_adiabatic_0.3_i

 Simulation Number  :   1

 Diagnostic         : OFF

 Iterations         :   1200

 Output Frequency   :   1200

 Time Dependence    : Steady
```

```
      ====================================
      Summary of 2D Axisymmetric Grid Data
      ====================================

      Total No. of nodes :    20900

      No. of line faces  :    41491

      Total No. of faces :    41491

      No. of quad cells  :    20592

      Total No. of cells :    20592

      ====================================
      Summary of Properties
      ====================================
      Total No. of Property VCs :       2
      ====================================
        ------------------------------
        Key No.          :        66
        Zone No.         :       1
        VC Name.         : NoName
        No. of Cells     :   12771
        Material  Type   : Fluid
        Density   method : Constant      = 2.70E+00
        Viscosity method : Constant_Dyn  = 9.36E-05
        Cond.     method : Prandtl       = 5.7E-01
        Sp. Heat  method : Constant      = 5.63E+03
        Absorbtion Coeff. Set : gas
        Emmissivity Set : None
        ------------------------------
        ------------------------------
        Key No.          :        67
        Zone No.         :       2
        VC Name.         : NoName
        No. of Cells     :    7821
        Material  Type   : Fluid
        Density   method : Constant      = 2.45E+01
        Viscosity method : Constant_Dyn  = 1.68E-05
        Cond.     method : Prandtl       = 7.1E-01
        Sp. Heat  method : Constant      = 2.24E+03
        Absorbtion Coeff. Set : fuel
        Emmissivity Set : None
        ------------------------------
      ====================================
    ================================================================
===============
                                              RAD_SNORD Statistics
    ================================================================
===============


              Radiation Parameters
```

```
Gray  model       = TRUE
CASN-DOM          = TRUE
S4  scheme        = TRUE
sn_hrange scheme  = TRUE


% Relative Error in Moments

     err_0m     = -2.980232E-06
     err_1m_mu  = -1.092752E-05
     err_1m_xi  = -1.092752E-05
     err_1m_et  = -1.000000E+02
     err_2m_mu  = -1.185405E-05
     err_2m_xi  = -1.185405E-05
     err_2m_et  = -1.185405E-05

No epsilon or length-scale provided at inlet
Epsilon reset to 0.01

  ====================================
 Summary of Geometry Data
 ====================================

 Smallest Volume   :   3.446387E-13

 Largest  Volume   :   2.670934E-09

 Smallest Angle    :   8.999974E+01 at face =       100

 Location of face number 100 is x =7.6200E-02 y =   1.3965E-04

 ==============================
 Start of Iterative Cycle.....
 ==============================

================================================================================
 Boundary-by-Boundary Mass Flow Summary (kg/sec/rad)
================================================================================
   Name        Key  Type        Inflow         Outflow        Sum
================================================================================
  2  gas       65  Outlet       0.000000E+00  -5.400326E-02  -5.40033E-02
  3  NoName    49  Interface    1.236721E-04  -1.236721E-04   0.00000E+00
  4  gas       64  Inlet        5.387959E-02   0.000000E+00   5.38796E-02
  6  fuel      63  Outlet       0.000000E+00  -1.351058E-02  -1.35106E-02
  8  fuel      62  Inlet        1.363425E-02   0.000000E+00   1.36343E-02
================================================================================
    Total volume source                                          0.00000E+00
================================================================================
================================================================================
    Total Mass Flow Summary     6.751384E-02  -6.751384E-02  -9.90540E-12
================================================================================
 Interfaces are not included in Total Mass Flow Summary.
================================================================================
```

```
================================================================================
 Boundary-by-Boundary Heat Transfer Summary (watts/rad)
================================================================================
 Name        key  Type     COND.+CONV.   W_SRC.+CVD   RADIATION*       Sum
================================================================================
gas           65  Outlet   -1.0558E+06   0.0000E+00   0.0000E+00  -1.0558E+06
gas           64  Inlet     1.0613E+06   0.0000E+00   0.0000E+00   1.0613E+06
fuel          63  Outlet   -2.0300E+04   0.0000E+00   0.0000E+00  -2.0300E+04
fuel          62  Inlet     1.5288E+04   0.0000E+00   0.0000E+00   1.5288E+04
wall          11  Wall     -1.4268E+01   0.0000E+00  -4.6446E+02  -4.7873E+02

================================================================================
 Total volume source                                                0.0000E+00
================================================================================
================================================================================

================================================================================
 Total Heat Imbalance      4.4783E+02   0.0000E+00  -4.6446E+02  -1.6630E+01
================================================================================
 Total wall HEAT source                                             0.0000E+00
* Radiation Summary Convention is +ve if  emmitting, -ve if absorbing.
* Cond+Conv Summary Convention is +ve if  flux into the cell, -ve if flux leavi
ng the cell.
================================================================================


 ============================
 End   of Iterative Cycle.....
 ============================

       Final Time   Elapsed Time=  9.963827E+03 Delta-time=  9.963827E+03
Normal Termination
```

LIST OF REFERENCES

1. Savur, Mehmet Koray, *A Numerical Study Of Combined Convective And Radiative Heat Transfer In A Rocket Engine Combustion Chamber,* Master's thesis, Naval Postgraduate School, Monterey, California, December 2002.

2. Modest, Michael F., *Radiative Heat Transfer*, McGraw Hill Inc., 1993.

3. Penner, S.S., Quantitative Molecular Speetroscopy and Gas Emissivities. Reading, Mass., Addison-Wesley, 1959.

4. Sutton, George P. and Biblarz Oscar, *Rocket Propulsion Elements*, John Wiley & sons, Inc, 7th Edition, 2001.

5. Sutton, George P., *Rocket Propulsion Elements: An Introduction to the Engineering of Rockets*, 6th Edition, John Wiley & sons Inc, 1992.

6. IMECE 2002: 2002 ASME International Mechanical Engineering Congress, "*Effects of Gas Radiation on the Thermal Characteristics of Regeneratively Cooled Rocket Engines*" by Mohammad H.N. Naraghi and Edmundo M. Nunes, November 2002.

7. CFDRC Research Corporation, *CFD-ACE User/Module Manual ,*Version 2002, 2003

8. Hill and Peterson, *Mechanics and Thermodynamics of Propulsion*, 2nd edition, Addison Wesley, 1992.

9. http://www.grc.nasa.gov/WWW/K-12/airplane/rockth.html, Glenn Research Center, NASA, November 2003.

10. http://www.chem.leeds.ac.uk/People/CMR/whatarescf.html,October 2003.

INITIAL DISTRIBUTION LIST

1. Defense Technical Information Center
   Ft. Belvoir, Virginia

2. Dudley Knox Library
   Naval Postgraduate School
   Monterey, California

3. Professor Gopinath
   Naval Postgraduate School
   Monterey, California

4. Professor Christopher Brophy
   Naval Postgraduate School
   Monterey, California

5. Director,
   Temasek Defence Systems Institute
   National University of Singapore
   Singapore

6. MAJ Goh Sing Huat Patrick
   Naval Postgraduate School
   Monterey, California